JOURNAL OF GEOPHYSICAL RESEARCH, VOL. 96, NO. D7, PAGES 13,033–13,065, JULY 20, 1991

Three-Dimensional Model Synthesis of the Global Methane Cycle

I. FUNG,[1] J. JOHN,[2] J. LERNER,[3] E. MATTHEWS,[3]
M. PRATHER,[1] L.P. STEELE,[4,5] AND P.J. FRASER[6]

The geographic and seasonal emission distributions of the major sources and sinks of atmospheric methane were compiled using methane flux measurements and energy and agricultural statistics in conjunction with global digital data bases of land surface characteristics and anthropogenic activities. Chemical destruction of methane in the atmosphere was calculated using three-dimensional OH fields every 5 days taken from *Spivakovsky et al.* (1990*a, b*). The signatures of each of the sources and sinks in the atmosphere were simulated using a global three-dimensional tracer transport model. Candidate methane budget scenarios were constructed according to mass balance of methane and its carbon isotopes. The verisimilitude of the scenarios was tested by their ability to reproduce the meridional gradient and seasonal variations of methane observed in the atmosphere. Constraints imposed by all the atmospheric observations are satisfied simultaneously by several budget scenarios. A preferred budget comprises annual destruction rates of 450 Tg by OH oxidation and 10 Tg by soil absorption and annual emissions of 80 Tg from fossil sources, 80 Tg from domestic animals, and 35 Tg from wetlands and tundra poleward of 50°N. Emissions from landfills, tropical swamps, rice fields, biomass burning, and termites total 295 Tg; however, the individual contributions of these terms cannot be determined uniquely because of the lack of measurements of direct fluxes and of atmospheric methane variations in regions where these sources are concentrated.

1. INTRODUCTION

Methane plays an important role in the Earth's radiative and chemical balance, yet its budget is not well known. While the major sources have been identified, there are considerable uncertainties in the source strengths [e.g., *Ehhalt*, 1974, 1985; *Ehhalt and Schmidt*, 1978; *Sheppard et al.*, 1982; *Khalil and Rasmussen*, 1983; *Blake and Rowland*, 1986, 1988; *Cicerone and Oremland*, 1988]. This uncertainty arises because of the paucity of measurements of methane emission. Also, methane fluxes vary widely as a result of the intrinsic heterogeneity of the landscape and political/economic/cultural factors. Flux measurements from a region span several orders of magnitude [e.g., *Sebacher et al.*, 1986; *Whalen and Reeburgh*, 1988]; extrapolation from individual flux measurements to a global budget is very difficult. The chemical loss of methane by reaction with tropospheric OH is not defined to better than ±25%, and the best estimates involve scaling to the lifetime of other gases such as methyl chloroform (CH_3CCl_3) [e.g., *Prinn et al.*, 1987; *Spivakovsky et al.*, 1990*a, b*]. A recent budget given by *Cicerone and Oremland* [1988] illustrates this uncertainty. They present a comprehensive survey and synthesis of our understanding of the methane cycle. Many sources are known individually only to a factor of 2. Better quantification of the sources and sinks must be made before we can understand and project the secular trend with confidence.

Information about the sources and sinks of methane is intrinsic in its atmospheric concentration and its variations. In addition to the globally averaged concentration and the annual rate of increase, additional source/sink information is contained in the north-south gradient and seasonal variations. Also, because each source or source group has a distinctive signature in ^{13}C, ^{14}C and deuterium, the geographic and temporal variations in the composition of these isotopes provide additional quantitative constraints on the budget of methane. Thus an indirect approach to study the atmospheric methane cycle would employ models of varying complexity to test the consistency between atmospheric methane variations and hypotheses about the sources and sinks. These models include globally averaged, height-dependent photochemical models for investigating the changing balance between sources and sinks [e.g., *Chameides et al.*, 1977; *Thompson and Cicerone*, 1986; *Quay et al.*, 1988], and photochemical-transport models in one, two, and three dimensions [e.g., *Mayer et al.*, 1982; *Crutzen and Gidel*, 1983; *Khalil and Rasmussen*, 1983; *Blake*, 1984; *Jones and Pyle*, 1984; *Fraser et al.*, 1986*a*; *Isaksen and Hov*, 1987; *Wahlen et al.*, 1989; *Quay et al.*, 1991; *Taylor et al.*, 1991]. The range of source strengths in these models corresponds to the range of estimates of chemical lifetimes of methane in the atmosphere. Furthermore, the magnitude and locations of the sources are tested in toto, and partitioning among the individual source terms using the indirect approach is not unique.

In this study, we present a synthesis of the global methane cycle in an attempt to derive a justified global budget of methane for the 1980s. Variations of methane and its isotopic composition in the atmosphere (section 2) are used to constrain hypotheses about the sources and sinks. We have embarked on an effort to map the geographic and seasonal distribution of all the major sources of methane. For a few of the sources (for example, wetlands) there is some information about their strengths as well as geographic distributions; while for other sources (for example, natural gas venting), geographic distribution can be deduced but direct estimates of the global source strength are difficult. A global three-dimensional tracer transport model (section 3) is used to simulate the atmospheric methane response to each of the sources and sinks (section 4). Candidate budgets that satisfy all the constraints (section 5) are

[1]NASA Goddard Space Flight Center, Institute for Space Studies, New York.
[2]Department of Applied Physics, Columbia University, New York.
[3]STX Corporation, New York.
[4]Cooperative Institute for Research in Environmental Sciences, Univ. of Colorado/NOAA, Boulder.
[5]Now at CSIRO Division of Atmospheric Research, Mordialloc, Victoria, Australia.
[6]CSIRO Division of Atmospheric Research, Mordialloc, Victoria, Australia.

Paper number 91JD01247.
0148-0227/91/91JD-01247$05.00

constructed, and the geographic and seasonal variations in the resultant atmospheric response are compared with the observations (section 6). By iteratively reducing the discrepancies between the observed and modeled distributions we converge on plausible methane budgets that are constrained by all the available methane observations. The three-dimensional distribution of methane in the atmosphere simulated for the preferred budget scenario is presented in section 7.

2. Observations of Atmospheric Methane and Its Isotopic Content

There now exists an extensive body of concentration measurements of atmospheric methane that may be used to gain insights into its global budget. Most of these measurements have been made by the technique of gas chromatography with flame ionization detection. Early surveys established the existence of a latitudinal gradient, with higher concentrations in the northern hemisphere [e.g., *Wilkness et al.*, 1973; *Lamontagne et al.*, 1974; *Ehhalt and Schmidt*, 1978; *Heidt et al.*, 1980]. Vertical profile measurements showed large decreases in concentration above the tropopause in the northern hemisphere [e.g., *Ehhalt and Heidt*, 1973] and increases in the troposphere in summer in the southern hemisphere [*Fraser et al.*, 1984, 1986*a*]. The existence of a seasonal cycle in methane concentration was first demonstrated by *Rasmussen and Khalil* [1981*a*]. The first papers which clearly documented an increase in atmospheric methane levels were published in the early 1980s [*Rasmussen and Khalil*, 1981*a*; *Fraser et al.*, 1981; *Blake et al.*, 1982]. Earlier, *Graedel and McRae* [1980] had suggested that global methane levels were increasing, but their analysis was based upon measurements of total hydrocarbons at urban/suburban sites, not on explicit measurements of methane. During the rest of the 1980s the body of information continued to grow [*Mayer et al.*, 1982; *Khalil and Rasmussen*, 1983; *Fraser et al.*, 1984, *Rasmussen and Khalil*, 1984*a*; *Fraser et al.*, 1986*a*; *Blake and Rowland*, 1986; *Steele et al.*, 1987; *Blake and Rowland*, 1988; *Khalil et al.*, 1989; *Hirota et al.*, 1989; *Dianov-Klokov et al.*, 1989*a, b*; *Zander et al.*, 1989; *Brunke et al.*, 1990].

The methane concentration data set used in this study is principally derived from the globally distributed cooperative flask sampling network of the Geophysical Monitoring for Climatic Change (GMCC) program of the National Oceanic and Atmospheric Administration (NOAA) [*Steele et al.*, 1987]. In 1989, reorganization within NOAA created the Climate Monitoring and Diagnostics Laboratory (CMDL), whose functions encompass those of the GMCC program. We shall employ the current nomenclature NOAA/CMDL here. We used data from 19 sites in this network, and these are listed in Table 1. This data set possesses several features crucial for the global simulations carried out in this study. First, the number of sampling sites is large and the sites are distributed widely over the surface of the Earth. Second, the frequency of flask sampling (approximately weekly) ensures that the major features of the seasonal variations are adequately defined. And third, the high precision (~0.2%) of the measurements and the fact that all flask samples are referenced against a single, well-

TABLE 1. Measurements Used for Comparison of Modeled and Observed Distributions of Atmospheric Methane

Station Code	Site	Latitude/Longitude		Years of Data Used	Position and Code in Model
		NOAA/CMDL Cooperative Flask Network Data			
ALT	Alert, NWT	82°N	62°W	1986-1987	
ASC	Ascension Island	8°S	14°W	1984-1987	1 gridbox south; AS1
AVI	St. Croix, Virgin I.	18°N	65°W	1984-1987	
AZR	Azores	39°N	27°W	1984-1987	
BRW	Pt. Barrow, Alaska	71°N	157°W	1984-1987	1 gridbox north; BR1
CBA	Cold Bay	55°N	163°W	1984-1987	
CGO	Cape Grim, Tasmania	41°S	145°E	1984-1987	
CHR	Christmas Island	2°N	157°W	1985-1987	
CMO	Capes Meares, Oregon	45°N	124°W	1984-1987	
GMI	Guam	13°N	145°E	1984-1987	
KEY	Key Biscayne, Florida	26°N	80°W	1984-1987	1 gridbox SE; KY1
KUM	Cape Kumukahi, Hawaii	20°N	155°W	1984-1987	
MBC	Mould Bay, NWT	76°N	119°W	1984-1987	
MLO	Mauna Loa, Hawaii	20°N	156°W	1984-1987	
NWR	Niwot Ridge, Colorado	40°N	106°W	1984-1987	
PSA	Palmer Station	65°S	64°W	1984,1985,1987	
SMO	American Samoa	14°S	171°W	1984-1987	
SPO	Amundsen Scott	90°S	25°W	1984-1987	
STM	Ocean Station "M"	66°N	2°E	1984-1987	
		CSIRO Data			
JBR	Jabiru, Northern Territory	13°S	133°E	1987-1989	1 gridbox SE; JB1
BAS	3.5-5.5 km, principally over Bass Strait, SE Australia	34-42°S	138-152°E	1982-1989	
		Other Data			
CPT	Cape Point, South Africa	34°S	18°E	1983-1988	
TKB	Tsukuba, Japan	36°N	140°E	1985-1987	

defined methane calibration scale provides confidence that the concentration gradients indicated by the data, and which we are attempting to simulate, are real. Full details of the methodologies used for obtaining methane concentrations from the NOAA/CMDL network, and the first 2 years of data, have been described by *Steele et al.* [1987]. Further details and additional data can be found in the works of Lang *et al.* [1990*a*, *b*]. The NOAA/CMDL methane data are also available as a numeric data package [*Steele and Lang*, 1991].

Methane data covering the 4-year period 1984–1987 are used in this work. For 16 of the 19 sites a complete 4-year record is available. Because of some gaps in the flask record, there are only three complete years (1984, 1985, 1987) of data for PSA (65°S) (cf. Table 1 for the explanation of the station codes and locations of the stations). Also, because of later starts in flask sampling, only three years (1985–1987) of data from CHR (2°N) and 2 years (1986–1987) of data from ALT (82°N) were used. For comparison with the model results the methane flask data have been processed to extract two major features.

The first feature of the methane data is the annual mean concentration at each site, averaged over the period of observations. To derive this quantity we first calculated, for each site, the annual mean concentration for each calendar year as the arithmetic mean of the monthly average values. Each monthly average concentration is itself the arithmetic mean of the individual flask values for that month [see *Steele et al.*, 1987]. Then to obtain the average annual mean concentrations for the period, the long-term growth rate of atmospheric methane must be removed from the data. To a very good approximation, the globally averaged growth rate of methane during this 4-year period was identical to the growth rate observed at SPO (90°S). Thus we subtracted the year-to-year growth increments seen at SPO from the annual means at each site, effectively normalizing all of the data to the annual average concentration measured at SPO in 1984. At all of the sites except for SPO, this procedure results in a set of detrended annual means which may then be averaged to obtain the average and standard deviation of the annual mean concentration.

The other feature derived from the data set is the average seasonal variation of atmospheric methane over a full year at each site. The procedure adopted here is the same for each site. The time series of monthly average methane concentrations were used to calculate 12-month running mean values. A least squares linear fit to the 12-month running means was determined and subtracted from the time series of monthly data. The detrended monthly values were then averaged by month, i.e., if there were 4 years of data for the site, all four of the detrended values for January were averaged, and so on for the other months. Average values and standard deviations were calculated.

Figure 1 shows the latitudinal and seasonal variations of atmospheric methane in the remote marine boundary layer derived from the NOAA/CMDL network. Annually averaged methane concentration is highest at BRW (71°N), which is 150 ppbv (parts per 10^9 by volume in dry air) above that of SPO (90°S). At the southern hemisphere middle- to high-latitude sites, methane peaks in September/October and minimizes in

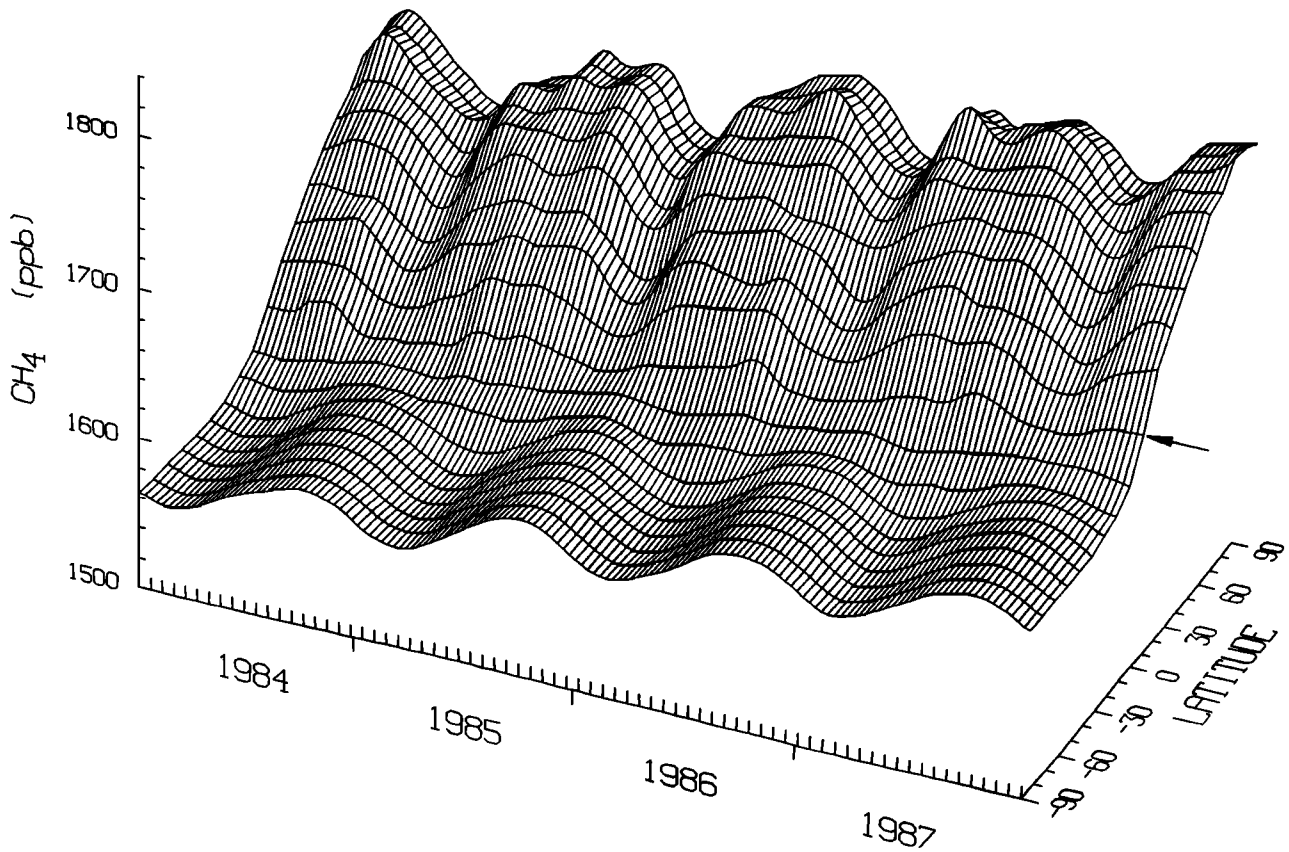

Fig. 1. Three-dimensional representation of the global distribution of the background concentration of methane measured in the marine boundary layer at the NOAA/CMDL cooperative flask network for 1984-1987. The arrow denotes the equator. The raw data have been smoothed to provide a uniform grid spacing of 10° in latitude and 10 days in time. See text and Table 1 for a discussion of the data used.

TABLE 2. The Average Seasonal Cycle and Annual Mean Methane Concentrations Measured at Monitoring Sites

	Jan.	Feb.	March	April	May	Jun.	Jul.	Aug.	Sep.	Oct.	Nov.	Dec.	AnnualAverage
ALT	14.70	9.73	22.47	6.94	3.45	-20.70	-26.57	-25.38	-11.59	10.90	12.91	6.35	142.70
	(8.53)	(1.66)	(11.67)	(8.31)	(0.03)	(5.06)	(9.27)	(9.96)	(11.06)	(14.04)	(4.54)	(12.13)	(0.57)
MBC	24.88	17.08	19.46	9.56	-2.42	-23.40	-28.24	-27.94	-12.38	7.66	6.81	10.22	145.03
	(6.22)	(11.85)	(4.29)	(4.78)	(3.47)	(4.18)	(2.45)	(3.06)	(5.96)	(10.50)	(8.33)	(1.82)	(5.62)
BRW	8.69	25.41	18.96	7.65	-7.37	-24.00	-29.34	-23.51	-5.35	15.66	4.37	5.15	149.98
	(9.65)	(13.38)	(14.93)	(8.05)	(5.27)	(5.08)	(11.47)	(6.57)	(8.87)	(25.46)	(9.80)	(4.80)	(4.02)
STM	11.13	3.23	18.46	7.58	-1.42	-12.31	-27.21	-19.47	-1.24	4.78	1.59	9.41	136.30
	(11.42)	(11.58)	(9.79)	(9.66)	(6.66)	(1.99)	(5.84)	(5.70)	(12.88)	(13.66)	(3.66)	(8.85)	(3.04)
CBA	8.67	9.25	11.47	10.29	1.80	-10.71	-27.63	-20.25	7.38	9.94	-2.58	3.35	135.53
	(9.06)	(10.84)	(7.10)	(3.36)	(5.03)	(7.29)	(7.57)	(4.30)	(9.46)	(6.50)	(6.02)	(4.64)	(2.90)
CMO	-5.03	-3.91	10.03	15.20	1.36	-5.75	-28.00	-27.75	-6.70	19.67	8.93	13.63	120.60
	(27.82)	(13.39)	(11.87)	(5.30)	(2.59)	(13.70)	(6.88)	(4.76)	(14.32)	(9.43)	(1.78)	(7.12)	(2.36)
NWR	0.52	9.76	16.95	0.20	5.29	-3.66	-23.04	-17.83	-12.53	11.46	8.09	9.22	95.43
	(13.45)	(12.62)	(6.40)	(6.99)	(7.85)	(4.39)	(10.35)	(9.21)	(9.59)	(5.48)	(6.58)	(8.32)	(2.28)
AZR	7.90	9.31	0.14	5.54	2.26	-11.38	-18.28	-18.29	-1.06	5.48	8.43	12.28	114.50
	(15.54)	(7.53)	(10.30)	(11.04)	(11.27)	(6.29)	(15.31)	(12.02)	(4.72)	(10.47)	(19.88)	(5.46)	(2.01)
KEY	25.83	14.14	3.54	20.91	-6.24	-19.54	-26.82	-27.55	-12.09	16.43	4.31	10.59	93.65
	(15.18)	(6.83)	(20.20)	(16.74)	(13.66)	(15.83)	(10.19)	(8.52)	(6.03)	(16.85)	(10.72)	(12.00)	(1.33)
MLO	2.09	0.72	0.12	6.16	0.80	-8.19	-14.43	-13.40	-4.80	6.46	14.69	7.38	62.03
	(3.95)	(6.05)	(16.53)	(7.89)	(5.94)	(7.79)	(13.80)	(4.31)	(14.19)	(3.18)	(9.35)	(4.22)	(0.74)
KUM	9.36	0.37	5.25	10.97	1.86	2.80	-21.60	-26.22	-4.59	4.49	5.60	8.72	81.98
	(18.96)	(9.36)	(8.82)	(7.91)	(16.85)	(9.28)	(6.59)	(8.20)	(10.93)	(6.73)	(6.62)	(9.21)	(3.11)
AVI	8.55	6.99	8.63	0.49	-4.31	-10.29	-12.60	-11.45	-14.47	-5.24	9.24	17.62	77.05
	(3.61)	(4.91)	(11.29)	(6.21)	(5.65)	(6.66)	(3.69)	(3.44)	(4.10)	(9.43)	(6.04)	(8.55)	(2.76)
GMI	6.97	18.90	16.86	7.75	-6.87	-11.80	-16.06	-22.89	-22.42	0.52	1.71	15.96	62.03
	(4.86)	(13.53)	(9.00)	(8.05)	(18.54)	(8.56)	(11.33)	(5.65)	(2.51)	(3.95)	(17.79)	(6.12)	(9.31)
CHR	8.72	1.16	19.95	21.53	5.74	-3.46	-7.28	-7.60	-10.20	-7.95	-6.83	-3.91	29.10
	(2.16)	(4.41)	(6.60)	(9.40)	(11.32)	(1.47)	(3.77)	(1.36)	(3.30)	(6.08)	(6.96)	(4.73)	(1.30)
ASC	-10.88	-13.67	-8.86	0.13	3.93	8.05	6.86	8.03	6.46	3.03	-1.11	-3.94	15.60
	(1.56)	(1.51)	(2.56)	(0.82)	(3.98)	(2.18)	(3.42)	(3.47)	(4.11)	(3.47)	(7.03)	(4.33)	(1.75)
JBR	-8.08	-8.69	-4.64	-5.04	-3.53	-1.93	5.93	7.74	8.65	8.79	1.22	0.78	*
	(8.19)	(2.28)	(1.94)	(2.24)	(0.96)	(0.63)	(1.09)	(4.88)	(4.56)	(0.74)	(6.80)	(14.27)	(*)
SMO	0.92	8.64	-1.42	-7.74	-4.77	-1.16	2.44	1.68	2.59	0.27	-4.10	-4.97	10.05
	(7.30)	(5.93)	(14.98)	(6.87)	(7.36)	(1.64)	(1.39)	(2.64)	(2.16)	(2.48)	(1.75)	(4.11)	(2.74)
CGO	-9.71	-15.48	-13.56	-10.30	-1.18	2.06	9.14	11.48	12.12	12.45	5.55	-1.37	1.88
	(1.07)	(1.02)	(1.45)	(2.44)	(2.94)	(1.77)	(2.00)	(1.93)	(1.14)	(1.19)	(1.28)	(1.47)	(0.31)
BAS	-9.35	-8.42	-5.18	-9.17	7.94	6.63	5.15	6.03	8.07	5.05	-2.00	-5.36	*
	(3.55)	(8.20)	(4.54)	(7.10)	(9.47)	(6.84)	(6.90)	(3.56)	(3.98)	(7.90)	(4.53)	(5.90)	(*)
PSA	-8.61	-15.81	-14.91	-10.45	-5.55	2.66	6.94	11.34	14.05	11.98	9.03	0.18	0.33
	(4.07)	(2.95)	(3.45)	(2.89)	(3.13)	(1.70)	(2.30)	(4.17)	(2.81)	(1.33)	(3.26)	(4.57)	(0.57)
SPO	-8.69	-14.72	-13.18	-10.15	-5.04	0.19	7.55	10.74	13.44	12.81	7.40	-0.50	0.00
	(1.23)	(2.41)	(2.82)	(1.57)	(1.84)	(1.52)	(1.25)	(3.43)	(1.90)	(0.77)	(0.47)	(1.23)	(0.00)

Refer to Table 1 for explanation of station codes (column 1) and period of data used. Seasonal cycles (columns 2-13) are defined with positive values denoting concentrations above the local annual mean. Averaged annual mean concentrations (column 14) are defined relative to the concentration at SPO. Numbers in parentheses denote $\pm 1\sigma$. Units are ppbv (parts per 10^9 by volume in dry air).

* Not intercalibrated against NOAA/CMDL data.

February, with a peak-trough amplitude of ~30 ppbv. At the northern hemisphere middle- to high-latitude sites, methane appears to show a complex double maximum in the year. It is clear that the average seasonal cycle is both simpler and better defined in the southern hemisphere than at most of the northern hemisphere sites. The annual mean concentrations and seasonal cycles averaged over the 4 years are given in Table 2.

In addition to observations from the NOAA/CMDL network we also used methane measurements made at two locations by the Commonwealth Scientific and Industrial Research Organization (CSIRO) Division of Atmospheric Research [cf. *Fraser et al.*, 1986*a*]; as well as at Cape Point, South Africa [*Brunke et al.*, 1990]; and at Tsukuba, Japan [*Hirota et al.*, 1989]. The CSIRO data are Jabiru, Northern Territory and from 3.5 to 5.5 km over Southeastern Australia. The monthly time series data at these sites were treated in the same way as the NOAA/CMDL data described above to obtain the annual mean and seasonal cycle at each site. The data were used to expand the observational base of the seasonal variation of atmospheric methane. However, as these data have not been precisely intercalibrated against the NOAA/CMDL data, they were not included in the analysis of the north-south gradient of atmospheric methane.

Data on isotopic content of atmospheric methane and the isotopic signatures of methane resulting from the production and destruction of methane by different processes provided additional information about the global methane cycle. These are summarized below.

A ^{14}C content of atmospheric methane of ~122 percent modern (pM) was reported for the northern hemisphere for 1987–1989 by *Wahlen et al.* [1989] and *Quay et al.* [1991]. In the southern hemisphere for the same period, both these studies reported values of 120–121 pM, close to the values reported by *Manning et al.* [1990]. The determination of the fraction of fossil sources in the global methane budget depends on the model and parameters used and is further complicated by uncertainties in $^{14}CH_4$ emission from pressurized water reactors. These ^{14}C values are interpreted as 16, 21, and 24.3% ^{14}C–free methane in the total emissions by *Quay et al.* [1991], *Wahlen et al.* [1989] and *Manning et al.* [1990], respectively. Uncertainties in these estimates are large, of the order of 9%. This fraction of fossil carbon is derived primarily from coal and natural gas sources and includes any methane from clathrate destabilization. Methane depleted in ^{14}C may also be derived from rice paddies, peat-rich wetlands and tundra. Direct measurements of $^{14}CH_4$ fluxes show close-to-modern methane emanating from these biogenic sources in North America [*Wahlen et al.*, 1989; *Quay et al*,. 1991]. Recent measurements show that the active layer of peat in Alaska has a ^{14}C age of only 1000–2000 years (D. Schell, personal communication, 1990). We therefore assumed in this study that rice paddies and wetlands make negligible contributions to the global emission of ^{14}C–depleted methane.

High-precision measurements of ^{13}C content of atmospheric methane have been made by several groups. *Stevens and Rust* [1982] reported values of –47.7±0.2 °/oo for both hemispheres in 1978–1983. More recently, globally averaged values of –46.7 °/oo for 1986–1987 were presented by *Wahlen et al.* [1989] and –47.2 °/oo for 1986–1989 by *Quay et al.* [1991]. *Stevens* [1988] and *Stevens and Engelkemeir* [1989] have found $^{13}CH_4$ trends at several stations in each hemisphere for the period 1978–1989. Also, an increasing $\delta^{13}C$ trend in the past 100 years has been determined from analysis of air bubbles trapped in Greenland ice cores [*Craig et al.*, 1988]. Because the sampling sites are few and the spatial variability of $^{13}CH_4$ in the atmosphere is unknown, we cannot evaluate if the reported values are hemispherically or globally representative. Also, the lack of intercalibration among these different data sets precludes the inference of a present-day trend from these values.

In this study, we relied on the $\delta^{13}C$ data of *Quay et al.* [1991]. Regular air samples were collected at Olympic Peninsula, Washington, and at MLO (20°N) and BRW (71°N), the latter two sites in collaboration with the NOAA/CMDL program. The samples were analyzed at a single facility at the University of Washington to produce time-series data on $^{13}CH_4$ that resolve seasonal variations over several years, and are referenced to the NOAA/CMDL methane concentrations at the same sites. These data are supplemented by data from sampling opportunities at CGO (41°S) and aboard NOAA research ships.

Central to the use of $\delta^{13}C$ of atmospheric methane in the analysis of the global budget is the value of $(k_{13}/k_{12})_{OH}$, the isotopic fractionation factor associated with OH oxidation. Values of 0.997 [*Stevens and Rust*, 1982], 0.990±0.007 [*Davidson et al.*, 1987], and 0.9946±0.0009 [*Cantrell et al.*, 1990] have been determined in different laboratory studies. The most recent values, those of *Cantrell et al.* [1990], are used here.

The $\delta^{13}C$ values of known methane sources and the kinetic fractionation between ^{13}C and ^{12}C which occurs during the oxidation of methane in soils have been measured in the field [e.g., *Rust*, 1981; *Stevens and Rust*, 1982; *Tyler*, 1986; *Tyler et al.*, 1988; *Quay et al.*, 1988; *Stevens and Engelkemeir*, 1988; *Chanton et al.*, 1988, 1989; *King et al.*, 1989; *Wahlen et al.*, 1989]. The reader is referred to *Tyler* [1989] for a review of the measurements. The values chosen in this study are discussed in section 6.

3. THREE-DIMENSIONAL ATMOSPHERIC TRACER TRANSPORT MODEL

The study of tracer distributions using a three-dimensional global general circulation model (GCM) was pioneered by *Mahlman and Moxim* [1978]. The tracer transport model employed in this study [*Russell and Lerner*, 1981] uses winds generated from the GCM at the Goddard Institute for Space Studies (GISS) [*Hansen et al.*, 1983] to advect and convect trace substances. Tracers, such as clorofluorocarbons (CFCs), CO_2, and CH_4, can be input at appropriate grid points, advected by model winds, and acted upon by specified sinks. The reader is referred to *Russell and Lerner* [1981], *Fung et al.* [1983], and *Prather et al.* [1987] for technical details of the model.

The version of the tracer model used in this study has realistic geography resolved at 4° latitude and 5° longitude and has 9 levels in the vertical. The 4°×5° version of the GCM simulates reasonably successfully the main features as well as higher-moment statistics of the atmospheric circulation. Full seasonal and diurnal cycles are resolved in the GCM. Four-hourly winds, convection, and rainfall statistics, as well as 5-day or monthly patterns of convective frequencies from the GCM were saved for use in the tracer model. In this study, circulation statistics from 1 year are used and are repeated for multiyear experiments.

The tracer model has been applied to the study of atmospheric distributions of CO_2 [*Fung et al.*, 1983; *Fung*, 1986; *Heimann et al.*, 1986; *Fung et al.*, 1987; *Tans et al.*, 1990], CO

[*Pinto et al.*, 1983], CFCs [*Prather et al.*, 1987], Krypton–85 [*Jacob et al.*, 1987], radon [*Jacob and Prather*, 1990] and methyl chloroform [*Spivakovsky et al.*, 1990*b*]. The studies published since 1987 used the same GCM circulation statistics as those used here and provide independent validation of the transport characteristics of the model. In particular, the interhemispheric exchange time of the order of 1.0 year is derived from the CFC and Kr–85 studies. Successful simulation of surface and aircraft measurements of the CO_2 annual cycle in both hemispheres [*Fung et al.*, 1987] validate to some extent the seasonal variations of vertical mixing in the model. Similarly, the agreement between observed and modeled seasonal patterns of CFCs and CH_3CCl_3, especially in the southern hemisphere, support the gross circulation statistics with regard to cross-equatorial tracer transport [*Spivakovsky et al.*, 1990*b*].

Although the tracer model is computationally more economical than the full GCM, the model at 4°×5° resolution takes ~2 hours CPU on the GISS Amdahl 5870 to simulate one tracer for one model year. A 3–4 year simulation is needed for the north-south gradient to stabilize (assuming an interhemispheric exchange time of 1.0 year). In order to facilitate a large number of model experiments we have made several simplifications to save computer time. First, a coarse-resolution model (8°×10°) was constructed using the winds and mixing parameters from the 4°×5° GCM. The coarse-resolution tracer model thus retains the circulation statistics of the 4°×5° GCM but uses ~22 min CPU per tracer year. Second, we note that the largest methane variations observed are small (150 ppbv pole to pole) compared with the global annual mean (1625 ppbv in 1984). Hence the methane simulations can be reduced to a quasi-linear problem, where the total response can be approximated by the linear sum of the responses to each of the source/sink functions. For sources, the linear approximation is exact; for chemical losses, or other sources/sinks which depend on the absolute atmospheric concentration, the error in such an approximation is at most ~10% of the signal. With such an approximation we can simulate separately the atmospheric response to a large number of hypotheses about each source/sink and examine their effects on the total atmospheric distributions in the diagnostic analyses after the model experiments. This will be discussed further in section 4.

Most of the measurement sites listed in Table 1 are in remote locations, far from continental sources and sinks. For these sites, modeled mean mixing ratios for the gridbox containing the sites are compared directly with the observations. For those sites located on continental coasts, air samples are taken from the "clean air sector," generally seaward of the site. We note that, for these coastal sites, direct comparison of model results and observations is invalid even if model concentrations are sampled according to wind direction, as the model gridboxes are large (4°×5° or 8°×10°) and must necessarily include local sources within the gridbox. We therefore used for comparison the modeled concentrations from a contiguous gridbox, in the direction of the clean air sector, which does not include any part of the continent. These are noted in Table 1; the station codes are modified to register the shift.

There is a problem in the location of the Intertropical Convergence Zone in the Atlantic Ocean in the GCM [*Druyan and Rind*, 1988, 1989] that affects the simulation at ASC (8°S). While ASC is observed to be influenced by southern hemisphere air, it is in the northern hemisphere circulation regime in the model. Since there is little latitudinal gradient in methane concentrations in the southern hemisphere [*Steele et al.*, 1987], the model results for the gridbox southward of ASC are used. In this way, interpretation of the methane simulations is not obfuscated by deficiencies in the meteorology in the GCM.

4. Methane Sources and Sinks and Their Atmospheric Signatures

A first step in using the geographic variation of atmospheric methane to infer sources and sinks is some knowledge of the patterns of the sources and sinks themselves. We have compiled, at 1°×1° resolution for the globe, a series of digital data bases of land surface characteristics and parameters important for the study of biogeochemical cycles. The primary data bases include vegetation and land use [*Matthews*, 1983], soils [*Zobler*, 1986], and countries and states [cf. *Lerner et al.*, 1988]. Built upon these are data bases of natural wetlands [*Matthews and Fung*, 1987], animal populations [*Lerner et al.*, 1988], rice cultivation [*Matthews et al.*, 1991], human population densities and associated activities such as municipal solid waste disposal. In addition, locations of coal mines, oil wells, and natural gas wells have been digitized from available atlases.

While we have relatively detailed information about source locations, making estimates of source strengths is difficult. For animals and natural wetlands, methane flux rates and seasons from a few measurement programs are extrapolated via these data bases to obtain the global distributions of methane emission. These are used directly in the simulations. Large uncertainties are associated with methane emissions from rice cultivation, landfills, natural gas production and consumption, coal mining, biomass burning, and termites. For these sources an arbitrary annual source strength, usually 10 or 50 Tg/yr (1 Tg = 10^{12} g), was chosen for mathematical and analytical convenience in the three-dimensional simulations. The model experiments and the source strengths used are listed in Table 3. Because of the linear decomposition discussed in section 3, atmospheric response to different source strengths or to a combination of sources can then be scaled proportionately. We shall use the shorthand WS(xx) to denote the case where results from experiment WS were scaled to a source strength of xx Tg/yr. In the construction of a global methane budget scenario (section 6), we held fixed the strengths of the better known sources and sinks, and varied the strengths of the lesser known ones until the combined atmospheric response satisfied all the constraints imposed by the atmospheric observations. In other words, the strengths of the sources and sinks are interdependent and are determined, in this study, from their combined signatures in the atmosphere.

A 4-year model experiment was run for each source scenario, by which time a stable north-south gradient in atmospheric methane is obtained in the model. Because emission rates are independent of the atmospheric concentration, each model experiment was started from a globally uniform background concentration of zero. The resultant increasing atmospheric concentrations were linearly detrended using the global, annually averaged growth rate in the experiment, thus preserving the geographic and seasonal variations of the simulated atmospheric distributions. The calculation of chemical destruction rates, which is dependent on the total methane concentration, is described separately in section 4.11.

To facilitate the analysis, the simulated three-dimensional distribution of methane concentration $\chi(\lambda,\theta,\sigma,t)$, is separated

TABLE 3. Summary of Three-dimensional Model Experiments Presented in This Study

Experiment	Source/Sink	Salient Emission Characteristics	Source Strength, Tg/yr		$\delta^{13}C$, °/oo
			Experiment	Expected*	Range†
		Sources			
W1	wetlands	five major wetland ecosystems; adhoc seasonality	110	100-200	-86 to -31
WB	bogs	forested and non-forested bogs; mainly 50°N-70°N; thaw cycle modeled	30		-85 to -50
WS	swamps	forested and non-forested swamps and alluvial formation; mainly tropical; wet season modeled	40	100-200	-73 to -31
WT	tundra	mainly 50°N-70°N; thaw cycle modeled	5		-73 to -55
RH	rice cultivation	mainly China and India; seasonal crop calendars; fixed emission per harvest	50	60-170	-68 to -58
AN	animals	subtropical/mid-latitudes; aseasonal	80	65-100	-76 to -45
LF	landfills	mid-latitudes; aseasonal	50	30-70	-56 to -46
GV	venting of natural gas at wells	mainly Middle East and West Siberia; aseasonal	50	25-50	-76 to -41
GL	pipeline leakage of natural gas	mid-latitudes; aseasonal	50		
CL	coal mining	mid-latitudes; aseasonal	50	25-45	-70 to -15
BB	biomass burning	tropical; dry season modeled	50	50-100	-32 to -24
TM	termites	tropical and subtropical; aseasonal	50	10-200	-76 to -54
HV	hydrate/clathrate	Soviet Arctic; aseasonal	10	?	
HZ	hydrate/clathrate	zonally symmetric; 76°-84°N	10	?	
		Sinks			
CH	chemical destruction	four-dimensional [OH] field	450	405-595	
SA	soil absorption	vegetation dependent; mainly mid-latitudes; aseasonal	50	5-58	

* Adapted from *Cicerone and Oremland* [1988] and *Born et al.* [1990].
† adapted from *Quay et al.* [1991].

into three components: G, the globally-averaged annual mean concentration; ϕ, the departure of the local annual mean concentration from G; and ξ, the departure of the local seasonal variation from ϕ:

$$\chi(\lambda,\theta,\sigma,t) = G + \phi(\lambda,\theta,\sigma) + \xi(\lambda,\theta,\sigma,t) \quad (1)$$

where λ is longitude, θ is latitude, σ is normalized pressure, and t is time. By definition,

$$\iiint \phi(\lambda,\theta,\sigma)\, d\lambda\, d\theta\, d\sigma = 0, \text{ and } \int \xi(\lambda,\theta,\sigma,t)\, dt = 0.$$

In other words, the global average of the annual mean concentration ϕ is zero, and annual integral of the seasonal variations ξ at each point is zero. From the linear detrending procedure, $G = 0$.

In the following we describe each of the methane sources/sinks used in the three-dimensional model experiments, and the simulated methane distribution in the lowest layer (σ corresponding to ~960 mbar) for each source or sink. The latitudinal distribution of the annual methane emission from each surface source/sink function is summarized in Table 4. For the stations listed in Table 1 we shall use the shorthand ϕ(STN) and ξ(STN,t), where STN is the station code, to denote the local annual mean and seasonal concentrations. For both model and observations, north-south profiles are defined relative to the South Pole, using ϕ(STN) − ϕ(SPO). For comparison, the simulated north-south profiles and seasonal cycles of atmospheric methane at the monitoring sites in response to the different sources are displayed in groups: seasonal sources (bogs, tundra, rice), predominantly northern hemisphere mid-latitude aseasonal sources (animals, landfills, natural gas production, natural gas consumption, coal mining) tropical sources (swamps and alluvial formations, biomass burning, termites), and arctic sources (clathrates).

4.1. *Natural Wetlands*

In our global digital data base of natural wetlands [*Matthews and Fung*, 1987], there are five major wetland ecosystems grouped according to characteristics important for methane emission: forested bogs, nonforested bogs, forested swamps, nonforested swamps, and alluvial formations. The global wetland area is 5.3×10^{12} m^2, with ~50% of this area occurring as forested and nonforested bogs between 50°N to 70°N. A data set of natural wetlands has also been compiled by *Aselmann and Crutzen* [1989] who obtained a global area of 5.7×10^{12} m^2, within 10% of ours. Relative regional distributions of areas are also very similar between the two works: their areas are ~6% higher between 50°N to 70°N and ~6% higher in the tropics. Given the scattered distribution of wetlands over most of the globe, agreement between the two data sets is considered good. The data set of *Matthews and Fung* [1987] was used in this study.

We investigated two hypotheses about the seasonal emission characteristics from wetlands and their impact on atmospheric methane variations. In experiment W1 the limited series of field measurements of emission rates published prior to 1987 were broadly extrapolated to represent emission rates for the entire wetland group. Peat-rich bogs were assumed to have "typical" emission rates of 0.2 g CH_4/m^2/d, while forested swamps and nonforested swamps were assumed to have lower

TABLE 4. Latitudinal Distribution of Annual Emission of Methane, Expressed as a Percentage of the Global Total for Each Source/Sink

Latitude	W1	WB	WS	WT	RH	AN	LF	GV	GL	CL	BB	TM	HV	HZ	SA
80°N-90°N	0	0	0	0	0	0	0	0	0	0	0	0	0	99	0
70°N-80°N	3	3	0	19	0	0	0	1	0	0	0	0	99	0	0
60°N-70°N	24	30	0	58	0	0	0	5	1	1	0	0	0	0	15
50°N-60°N	27	36	3	20	0	11	13	4	26	16	0	3	0	0	19
40°N-50°N	9	11	7	1	1	16	34	4	36	27	0	4	0	0	14
30°N-40°N	2	2	2	0	13	13	29	17	22	34	0	8	0	0	11
20°N-30°N	2	2	2	0	47	18	9	39	7	10	9	9	0	0	5
10°N-20°N	5	0	8	0	19	9	3	4	2	1	24	12	0	0	6
0°-10°N	6	2	16	0	5	6	1	9	1	0	25	16	0	0	4
10°S-0°	6	8	24	0	7	3	1	5	0	0	22	15	0	0	4
20°S-10°S	5	1	11	0	1	6	0	0	0	0	14	15	0	0	8
30°S-20°S	4	0	13	0	2	6	1	2	0	4	2	10	0	0	4
40°S-30°S	1	0	8	0	0	5	2	2	1	3	0	2	0	0	2
50°S-40°S	0	0	0	0	0	1	0	1	0	0	0	0	0	0	0
60°S-50°S	0	0	0	0	0	0	0	0	0	0	0	0	0	0	0
70°S-60°S	0	0	0	0	0	0	0	0	0	0	0	0	0	0	0
80°S-70°S	0	0	0	0	0	0	0	0	0	0	0	0	0	0	0
90°S-80°S	0	0	0	0	0	0	0	0	0	0	0	0	0	0	0
Global	100	100	100	100	100	100	100	100	100	100	100	100	100	100	100

See Table 3 for explanation of the codes and expected range of global strengths of the sources.

emission rates of 0.07 and 0.12 g $CH_4/m^2/d$, respectively. Also, simple assumptions were made about emission seasons: emission periods were 180 days at the equator and decreased monotonically polewards to 100 days at 70°N. An estimated annual emission of 110 Tg was obtained. This was presented in the work by *Matthews and Fung* [1987] and used in the *Cicerone and Oremland* [1988] budget analysis. We have included here an additional seasonal emission of 5 Tg from dry tundra, as postulated by *Whalen and Reeburgh* [1988].

In the past few years there has been an increase in field measurements of methane emission from wetland ecosystems, so that a better treatment is now feasible. Results from the Amazon Boundary Layer Experiment (ABLE IIA) show emission rates from the Amazonian floodplains that are higher than previously assumed [*Harriss et al.*, 1988; *Crill et al.*, 1988*a*; *Bartlett et al.*, 1988]. On the other hand, preliminary results from the 1988 Arctic Boundary Layer Experiment (ABLE IIIA) show lower fluxes from Alaskan wetlands than those found by *Sebacher et al.* [1986]. The low values are consistent with those measured by *Svensson* [1981], *Svensson and Rosswall* [1984] and *Moore et al.* [1990]. Measurements from Minnesota wetlands show fluxes from forested bogs to be of the same order as those found from ABLE IIIA, while the fluxes from open bogs were found to be an order of magnitude higher [*Crill et al.*, 1988*b*]. For these bogs a clear temperature dependence of the fluxes was found. Furthermore, the time series data of *Whalen and Reeburgh* [1988] show a clear seasonal cycle in methane emission: emission from tundra sites in Alaska begins in June/July, reaches a maximum in August, and ceases by November.

For this study we modeled both emission seasons and emission rates based on the climatology of monthly surface air temperatures (*Ts*) and precipitation [*Shea*, 1986]. The modeling was carried out separately for bogs (experiment WB), swamps/alluvial formations (experiment WS), and dry tundra (experiment WT).

Most wetlands experience seasonal wet/dry cycles and/or freeze/thaw cycles. In our model, methane is emitted only during wet and/or thaw seasons. For a location that experiences above freezing temperatures throughout the year, wet season was assumed to occur when monthly precipitation exceeds monthly potential evaporation. Potential evaporation is the maximum demand for moisture and is calculated from *Ts* using Thornthwaite's formula (1948). Thaw season was assumed to begin when monthly mean *Ts* rises above 5°C and assumed to end when monthly mean *Ts* falls below 0°C. The *Ts* criteria for freeze/thaw were chosen to match the observations of *Whalen and Reeburgh* [1988] at the University of Alaska site. With this definition, the duration of methane emission ranges from 12 months per year at the headwaters of the Amazon River to 5 months at its mouth, and from 6 months in the maritime south coast of Alaska to 4 months on the north coast.

It remains to determine the variation of emission rates during the emission season. Seasonal time series of methane fluxes from tussock and carex sites in Alaska [*Whalen and Reeburgh*, 1988] show that methane emission rates appear to peak with *Ts* in August. We therefore assumed, as a first approximation, that methane emission rates for forested and nonforested bogs in experiment WB are temperature-regulated. The temperature dependence is assumed as:

$$k(Ts) = k(To) * Q_{10}^{(Ts-To)/10} \quad (2)$$

We assumed $Q_{10}=2$ and $k=0.05$ g $CH_4/m^2/d$ at $To=10$°C. Equation (2) gives a flux of 0.07 and 0.1 g $CH_4/m^2/d$ for $Ts=15$°C and 20°C, respectively. This is within the range of the tussock data of *Whalen and Reeburgh* [1988] which show peak fluxes of 0.03, 0.09, and 0.16 g $CH_4/m^2/d$ for three tussock sites in July/August when $Ts\sim15$°C. It approximates the flux reported for ombrotrophic forested bogs in Minnesota in May-June ($Ts\sim15$°C) and is half that for Minnesotan fens and open bogs where hydrology and substrate quality play an important role in determining methane emissions [*Crill et al.*, 1988*b*]. The global source in experiment WB is thus estimated to be 30 Tg/yr.

While the emission season of tropical wetlands is based on wet/dry seasons, there are little data on seasonal variations of the methane flux itself. In experiment WS, which investigates emissions only from forested and nonforested swamps and from alluvial formations, we assumed a constant methane flux throughout the emission season. The emission rate is assumed to be 0.07, 0.12, and 0.20 g $CH_4/m^2/d$ for forested swamps, nonforested swamps, and alluvial formations, respectively, based on the data of *Crill et al.* [1988*a*], *Bartlett et al.* [1988], and *Devol et al.* [1988, 1990]. The total emission from swamps and alluvial formations is calculated to be 40 Tg CH_4/yr. Because of the wide range of fluxes reported for tropical wetlands, we consider the emission from this source to be highly tentative.

Whalen and Reeburgh [1988] report there are low levels of methane fluxes, ~0.005 g $CH_4/m^2/d$ emanating from the dry tundra. Because of the large expanse of tundra area, 7.2×10^{12} m^2, this source adds up to ~5 Tg/yr (experiment WT).

With the inclusion of emissions of 5 Tg from the dry tundra the global methane emission from wetlands is 115 Tg in experiment W1 and 75 Tg by summing WB, WS, and WT. Emission from bogs is 75 Tg in W1 and 30 Tg for WB; that from swamps and alluvial formations is 35 Tg in W1 and 40 Tg in WS. The combined emission pattern of global wetlands from WB, WS, and WT has two comparable annual emissions maxima centered around 50°N to 70°N and 20°S to 20°N.

The annual mean distribution $\phi(\lambda,\theta)$ at ~960 mbar is shown in Figures 2*a*–2*d* for experiments W1(110), WB(30), WS(50), and WT(5), respectively. Although a direct extrapolation of the flux measurements yielded an annual source of 40 Tg CH_4/yr for WS, we display here the atmospheric response to WS(50) for comparison with other tropical sources. In general, the near-surface atmospheric distributions reflect the locations of the major wetlands of the world. In experiment W1(110), concentrations > 50 ppbv above the global mean are simulated over the wetlands of Alaska and the Hudson Bay lowlands, whereas in WB(30), where the bog emission is reduced by at least a factor of 2 compared to experiment W1(110), the elevation is only ~18 ppbv. The concentration elevation is > ~70 and ~25 ppbv above the Siberian lowlands in W1(110) and WB(30), respectively. In WS(50) the wetlands of South America lead to an elevation of ~15 ppbv above the global mean.

The annual mean north-south gradient simulated at the monitoring sites in the marine boundary layer is shown in Figure 3*a* for WB(30) and WT(5) and in Figure 3*c* for WS(50). The annual mean concentration at each of the observing sites is plotted relative to that at SPO (90°S). As is expected from the wetland distribution, concentrations are highest at BRW (71°N) for WB, and at MBC (76°N) for WT. In WB(30), northern hemisphere high-latitude sites are elevated by as much as 8 ppbv above the mid-latitude sites, which in turn are higher than the southern hemisphere by ~15 ppbv.

Similar patterns are found for WT(5) where ϕ(ALT) – ϕ(SPO) is ~6 ppbv. By comparison, emissions from WS(50) are mainly from the southern hemisphere tropics, and so the NOAA network would register a peak concentration at SMO (14°S) and ASC (8°S) of ~4 ppbv above that at SPO (90°S). There is very little concentration difference between the hemispheres.

The peak-trough amplitudes of the seasonal cycles resulting from wetland emissions are illustrated in Figure 4*a* for W1(110). Because of the large emission rates and short emission period, the seasonal cycle is most pronounced at BRW (71°N), where the peak-trough amplitude is ~130 ppbv, and decreases southward, with an amplitude of ~60 ppbv at CMO (45°N), ~24 ppbv at KUM (20°N), ~9.5 ppbv at SMO (14°S)

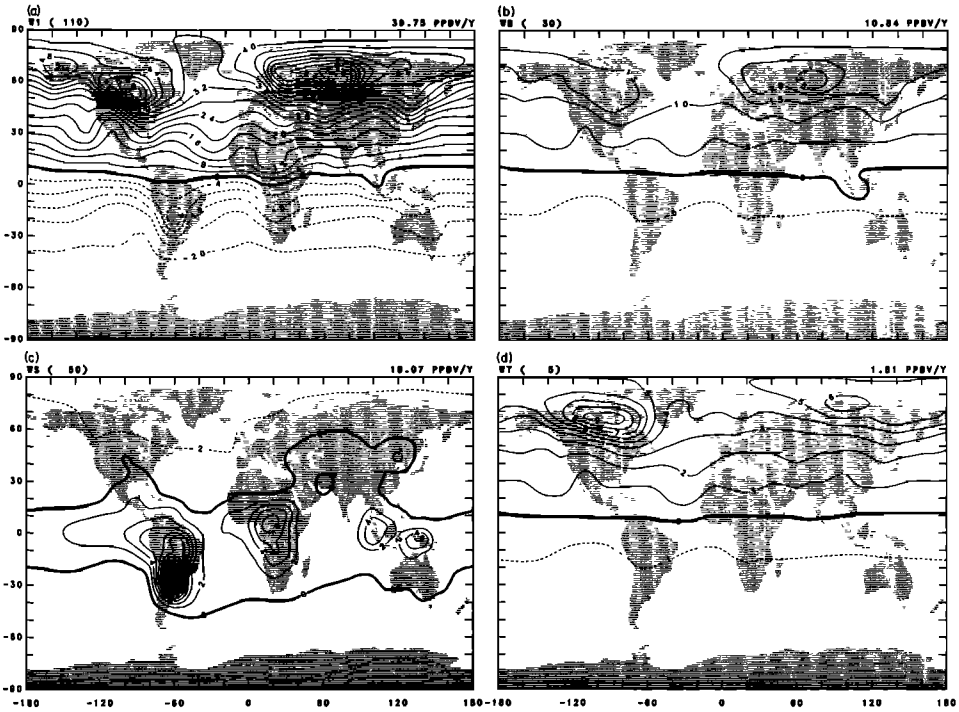

Fig. 2. Latitude-longitude distributions of the annual mean methane concentration $\phi(\lambda,\theta)$ simulated in the first layer (~960 mbar) of the model for each of the experiments: (*a*) W1(110); (*b*) WB(30); (*c*) WS(50); (*d*) WT(5); (*e*) RH(50); (*f*) AN(80); (*g*) LF(50); (*h*) GV(50); (*i*) GL(50); (*j*) CL(50); (*k*) BB(50); (*l*) TM(50); (*m*) HV(10); (*n*) HZ(10); (*o*) CH(-450); (*p*) SA(-50). See text and Table 3 for explanation of the experiments. Concentrations are defined relative to the global annual mean, and dashed lines denote negative values. Units are ppbv.

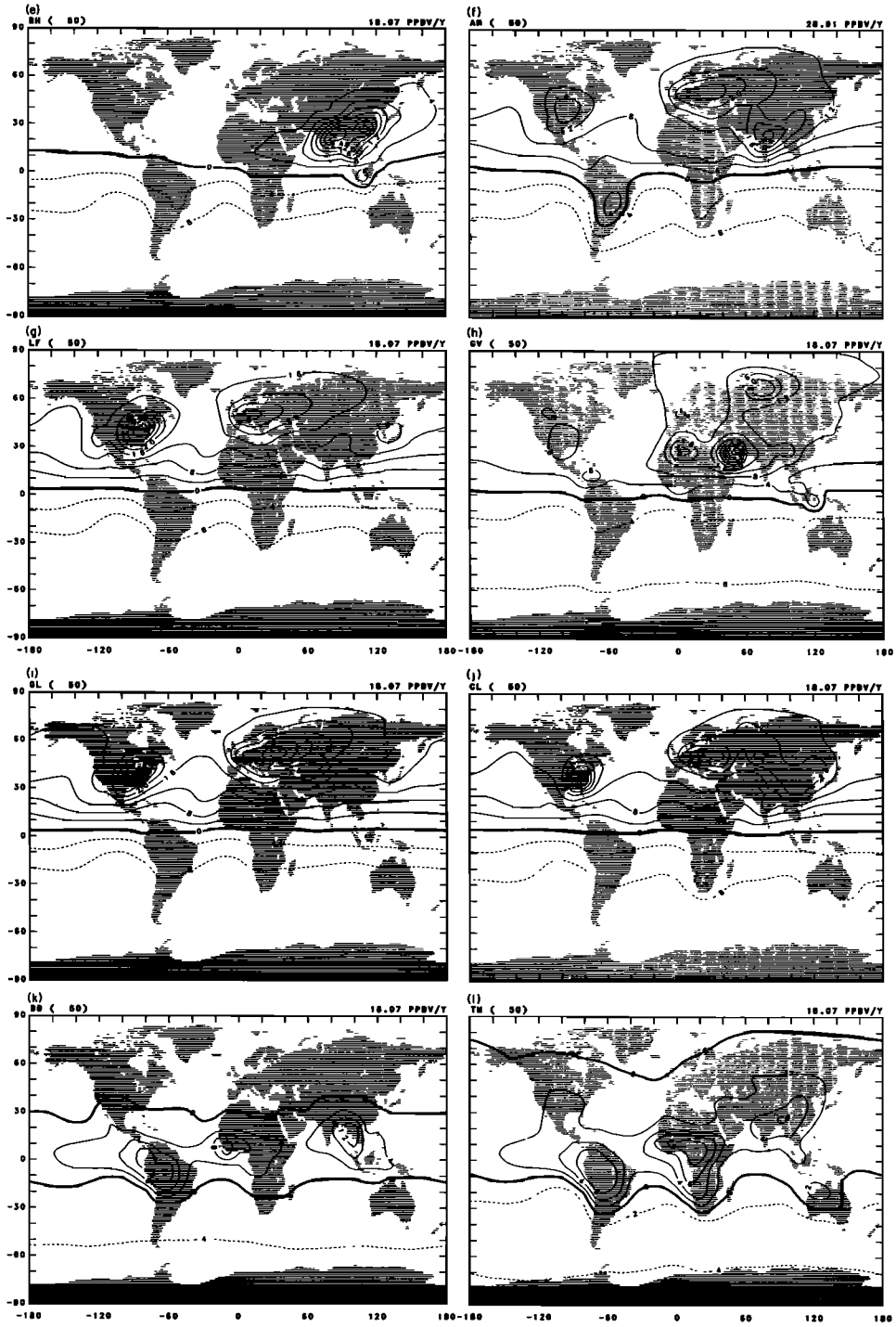

Fig. 2. (continued)

and ~8 ppbv at CGO (41°S). The maximum concentration occurs at the end of the emission season assumed: September at BRW (71°N), around September/October at CMO (45°N), November at KUM (20°N), January at SMO (14°S), and April at CGO (41°S).

For WB(30) the largest amplitude, ~40 ppbv, is also found at BRW (71°N). The amplitude decreases to ~20 ppbv at mid-latitudes in the northern hemisphere and to ~2 ppbv in the southern hemisphere. The seasonality for WT(5) is correspondingly reduced, but the amplitudes at BRW (71°N) and MBC (76°N) remain large, ~25 ppbv.

4.2. *Rice Paddies*

Flooded rice fields, like natural wetlands, are anaerobic environments favorable for methane production. Likewise, methane emissions from rice paddies are affected by local environmental, edaphic, phenological, and ecological variations. Furthermore, the type of fertilizer applied can enhance or depress the flux escaping to the atmosphere *(Schütz et al.*, 1989; *Yagi and Minami,* 1990]. Measurements of methane emission from rice paddies at mid-latitude research sites [*Cicerone and Shetter*, 1981; *Cicerone et al.*, 1983; *Holzapfel-Pschorn and Seiler,* 1986; *Schütz et al.*, 1989; *Sass et al.*, 1990] yield a total emission

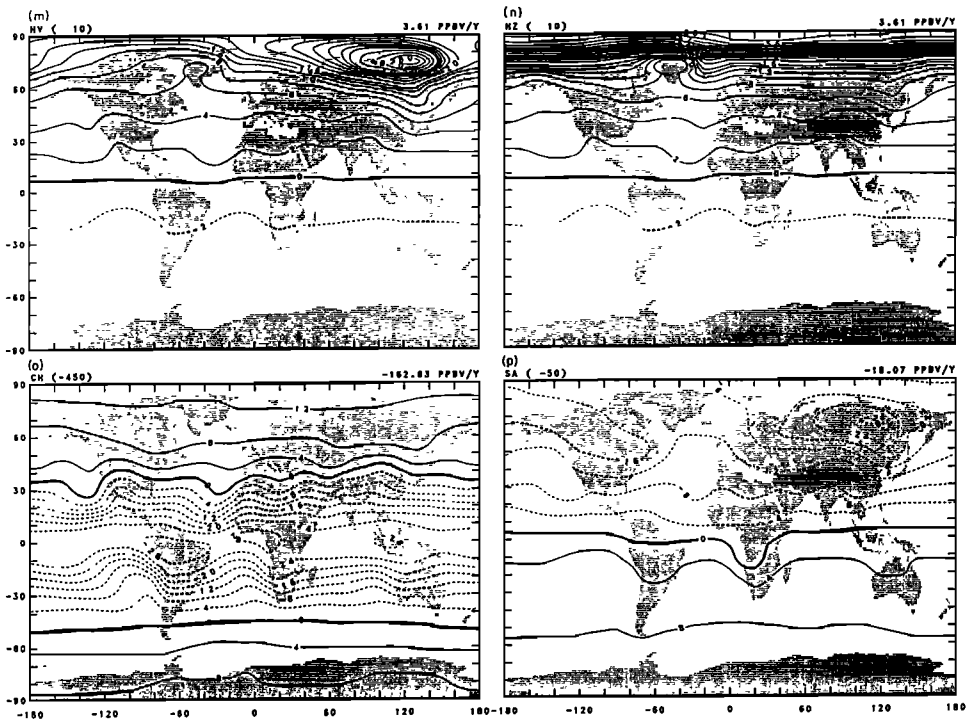

Fig. 2. (continued)

of 5–54 g CH_4/m^2 for each harvest cycle, with the fluxes within a growing season varying with plant phenology and agricultural practices. Recent measurements in Hangzhou, China [*Schütz and Seiler*, 1989; *Schütz et al.*, 1990] give emission rates as high as 38 mg/m^2/h, or 90 g CH_4/m^2 for a growing season of 100 days. In 1984 the global rice harvest area was 1.5×10^{12} m^2 [*Food and Agriculture Organization*, 1985]. If all the area were emitting methane, the annual emission would range from 35–220 Tg/yr. Such large site to site variability makes global extrapolations very uncertain.

We have compiled a digital data base of rice cultivation at 1°×1° resolution [*Matthews et al.*, 1991]. A total of 103 countries grew rice in 1984, with China and India together accounting for 52% of the global harvest area [*FAO*, 1985]. For each country we extracted from the literature the number of rice harvests in a year, the timing of each harvest, and the area of each harvest. The reader is referred to *Matthews et al.* [1991] for a detailed description of the data. Total rice harvest area, its geographic distribution, and the seasonal pattern of methane emission are similar to the temperature-dependent estimate of *Aselmann and Crutzen* [1989].

Even with the monthly distribution of rice cultivation area, it is difficult to estimate the corresponding seasonal methane emission, as we cannot quantify globally the factors that control intraharvest and among-site variations of methane emission. We carried out a sensitivity experiment to investigate how rice emissions impact atmospheric methane distributions. In this experiment, RH, a global annual emission of 50 Tg/yr was assumed for mathematical convenience, so that the total emission per harvest cycle was constant at 34 g CH_4/m^2. Thus the daily emission rates range from 0.16 g $CH_4/m^2/d$ for the 7-month growing season in Malagasy to 0.38 g $CH_4/m^2/d$ for the 3-month season for second crops in Taiwan and the Philippines. These emission rates are in the range of the measurements of *Cicerone et al.* [1983], *Holzapfel-Pschorn and Seiler* [1986], and *Schütz et al.* [1989, 1990].

Figure 2*e* shows the annually averaged near-surface distribution $\phi(\lambda,\theta)$ of methane simulated for RH(50). Concentrations are elevated above background values by ~16 ppbv at TKB (36°N) and ~25 ppbv over India and China. By contrast, except at GMI (13°N), the concentration in the northern hemisphere NOAA/CMDL sites is elevated by only ~3 ppbv.

Because of the remoteness of the monitoring sites from the source regions, the north-south gradient simulated at the NOAA/CMDL sites for RH(50) is about half that for WB(30) (Figure 3*a*). The concentration is relatively high at middle latitudes in the northern hemisphere, ~13 ppbv above SPO (90°S), and decreases sharply by ~7 ppbv from GMI (13°N) to SMO (14°S). In RH(50) the simulated peak-trough amplitudes are ~8 ppbv at the northern hemisphere sites and ~3 ppbv in the southern hemisphere (Figure 4*a*).

We also carried out a sensitivity experiment where the daily emission is constant at 0.25 g $CH_4/m^2/d$ throughout the growing season to yield an annual total emission of 50 Tg/yr. In this experiment the total emission is larger for a long growing season (mainly for single-crop systems) than for a short growing season. The simulated distributions at the monitoring sites are practically indistinguishable from those in experiment RH(50).

4.3. *Animals*

Methane is produced by enteric fermentation in animals, mainly ruminants. We have applied emission rates cited by *Crutzen et al.* [1986] to our global data bases of animal populations to obtain the global distribution of methane emissions from animals [*Lerner et al.*, 1988]. The global emission rate was 78 Tg in 1984. Because of the economic importance of animal husbandry, this is one of the better known sources in the methane budget; the uncertainties in the magnitude and distribution of this source have been emphasized by *Crutzen et al.* [1986] and *Lerner et al.* 1988]. We carried out

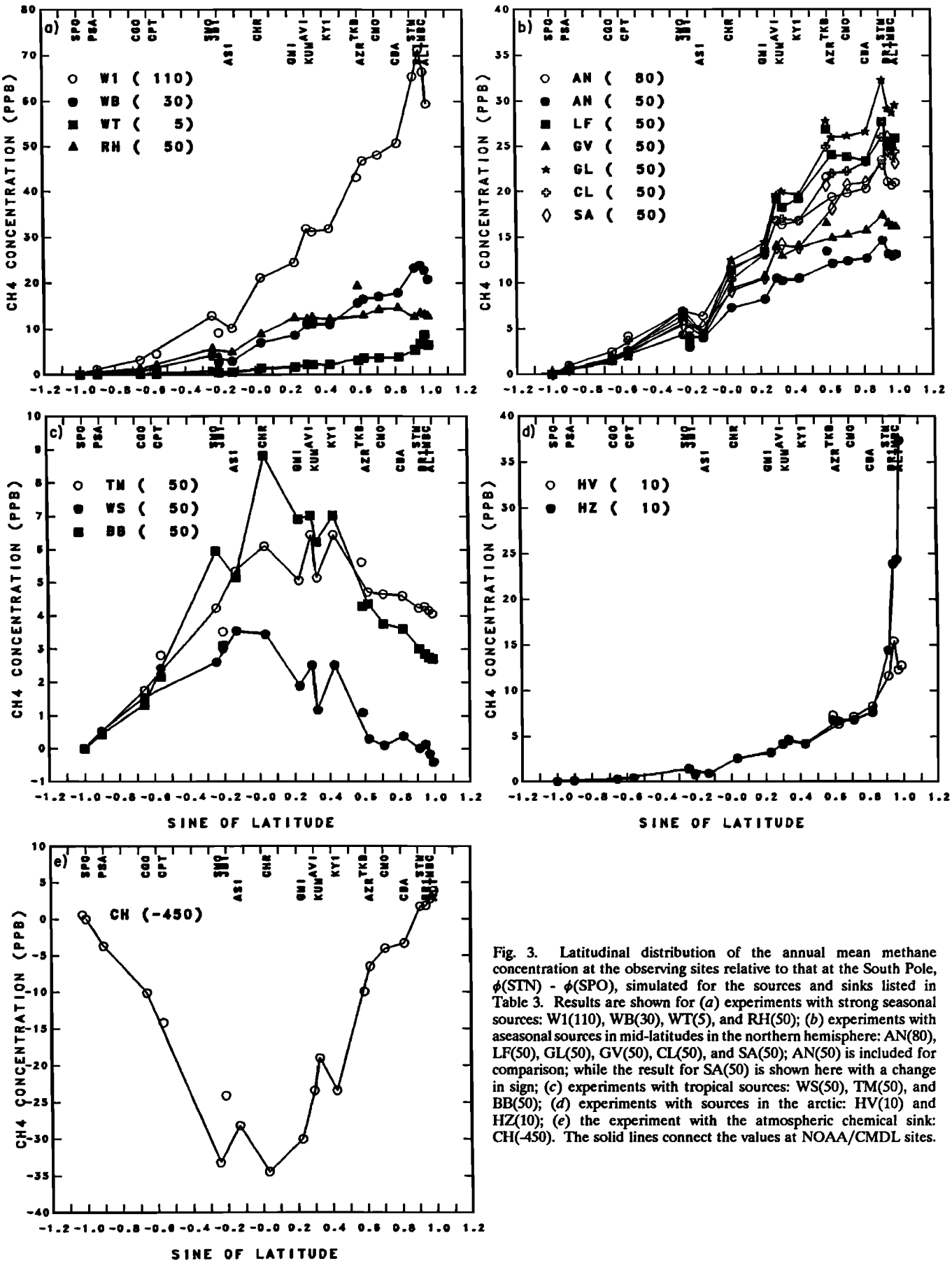

Fig. 3. Latitudinal distribution of the annual mean methane concentration at the observing sites relative to that at the South Pole, ϕ(STN) - ϕ(SPO), simulated for the sources and sinks listed in Table 3. Results are shown for (*a*) experiments with strong seasonal sources: W1(110), WB(30), WT(5), and RH(50); (*b*) experiments with aseasonal sources in mid-latitudes in the northern hemisphere: AN(80), LF(50), GL(50), GV(50), CL(50), and SA(50); AN(50) is included for comparison; while the result for SA(50) is shown here with a change in sign; (*c*) experiments with tropical sources: WS(50), TM(50), and BB(50); (*d*) experiments with sources in the arctic: HV(10) and HZ(10); (*e*) the experiment with the atmospheric chemical sink: CH(-450). The solid lines connect the values at NOAA/CMDL sites.

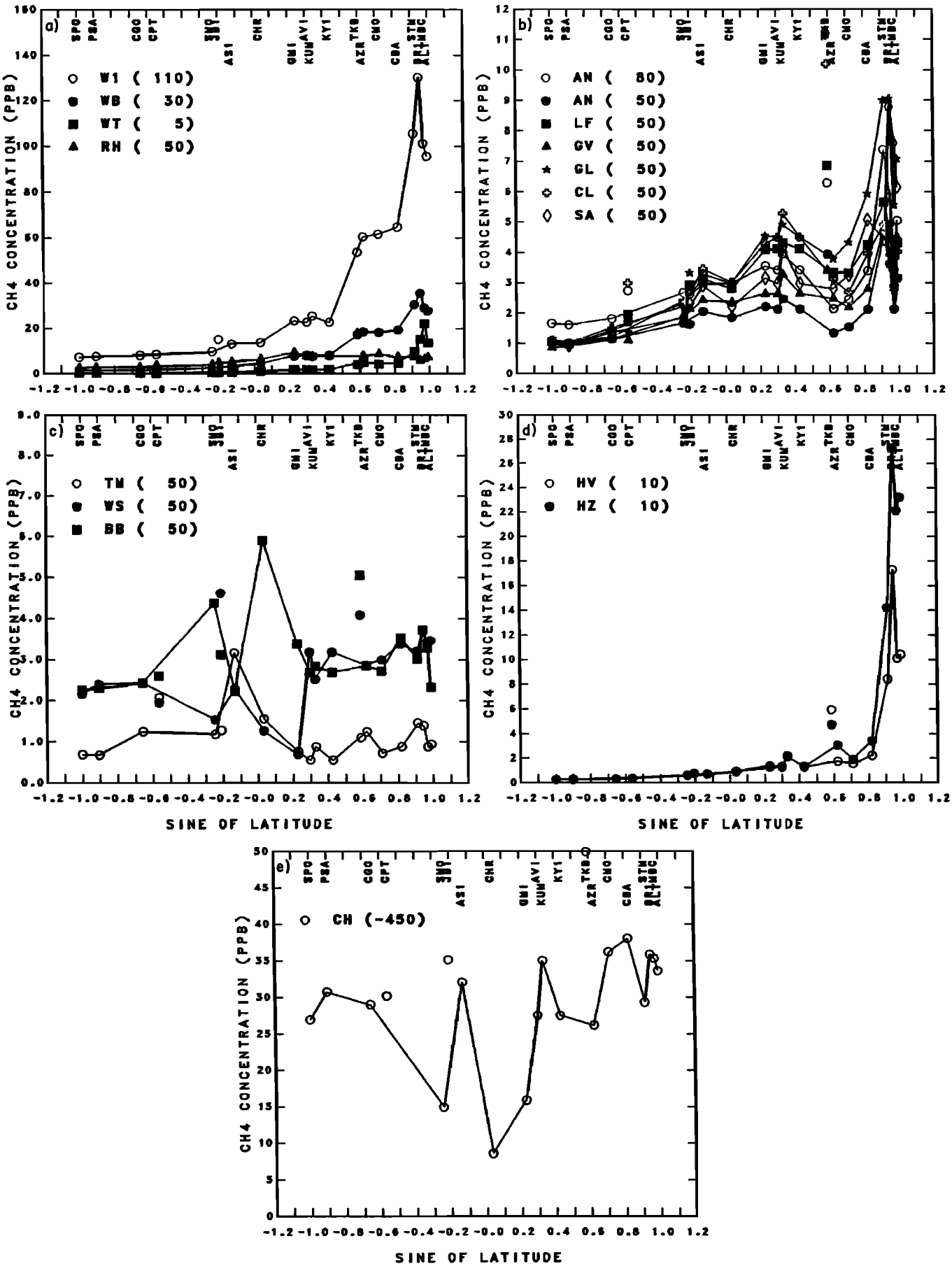

Fig. 4. Like Figure 3, but for peak-trough amplitudes of the methane seasonal cycles $\xi(\mathrm{STN},t)$ simulated at the observing sites.

only one experiment, AN(80), with this source and assumed that the emission is aseasonal.

In Europe and South Asia where there are high densities of cattle, dairy cows, and water buffalo, the simulated surface methane concentration is >20 ppbv above the global mean (Figure 2*f*). The central plains of North America and the Sudeste (southeastern) region of Brazil, both with high cattle populations, also exhibit elevated surface methane concentrations. The north-south profile of annual mean methane concentration simulated at the NOAA/CMDL sites is shown in Figure 3*b* for AN(80). The results for AN(50) are included for comparison with other aseasonal mid-latitude sources. For AN(80), fairly uniform methane concentrations (~20 ppbv higher than the South Pole) are simulated in mid-latitudes in the northern hemisphere, and the concentration decreases monotonically toward the South Pole. As may be expected from an aseasonal source, intra-annual fluctuations in methane concentration due to seasonally varying circulation patterns are small (Figure 4*b*). The peak-trough range of methane oscillation due to this source is ~5 ppbv for the NOAA/CMDL sites in middle to high latitudes in the northern hemisphere, ~4 ppbv in the tropics and subtropics (KUM (20°N), SMO (14°S), ASC (8°S)), and ~2 ppbv at CGO (41°S).

4.4. *Landfills*

Anaerobic environments may be found in landfills that are several years old. Decomposition of biodegradable organic material in these landfills produces carbon dioxide and methane which may escape to the atmosphere. *Bingemer and Crutzen* [1987] have made a survey of the production of municipal and industrial waste and the biodegradable carbon content of the waste. Assuming that the methane proportion of landfill gas is constant and that all the methane in landfill gas escapes to the atmosphere, they estimated the global production of methane in landfills to be 30–70 Tg CH_4/yr. The amount of methane that escapes to the atmosphere may vary from site to site, and may depend on, inter alia, the carbon content of the landfill and the porosity of the cover. Explosive levels of methane have been found at some sites (C. Moore, personal communication, 1988), while undecomposed organic material is found at others [*Rathje*, 1989]. Methane consumption in landfill cover soil also reduces the emissions [*Whalen et al.*, 1990]. *Bingemer and Crutzen* [1987] expect the emission estimates to be lower than the production estimates of 30–70 Tg. Most of the methane from landfills is from North America, where both the per capita production of municipal solid waste and the biodegradable fraction of the waste are high.

We combined our global data base on human population densities with per capita statistics on biodegradable carbon given by *Bingemer and Crutzen* [1987] for different regions to produce a global map of methane emission from landfills. For comparison with other sources, a global source strength of 50 Tg/yr is used in experiment LF.

The atmospheric methane distribution resulting from this source is shown in Figure 2*g*. Because of the high production of biodegradable carbon, surface methane concentrations are >30 ppbv above the surface mean over the large population centers in Northeastern U.S.A. and Eastern Canada and >25 ppbv over Western Europe. By contrast, the surface concentration is elevated by only ~12 ppbv over China, with approximately equivalent population densities.

The north-south gradient simulated at the NOAA/CMDL sites is typical of northern hemisphere mid-latitude sources (Figure 3*b*). For a source of 50 Tg the annually averaged concentration at middle to high latitudes in the northern hemisphere is elevated by ~25 ppbv relative to SPO (90°S). The sharpest gradient, ~15 ppbv, is found between KUM (20°N) and SMO (14°S). With this aseasonal source the seasonal fluctuations at the NOAA/CMDL sites caused by seasonal circulation are ~4 ppbv in the northern hemisphere and ~1 ppbv in the southern hemisphere (Figure 4*b*).

4.5. *Natural Gas Production*

In 1984 global gross production of natural gas was 71,963 billion cubic feet and marketable production was 62,382 billion cubic feet [*U.S. Department of Energy*, 1986*a*]. Methane content of natural gas is on average 90% and so the marketable production figures are equivalent to ~1200 Tg CH_4/yr. Thus any escape of natural gas during production and consumption processes may be a significant source of atmospheric methane. Natural gas can escape during several production stages, the most significant of which is associated with venting at oil and natural gas wells. Other venues such as escape during field exploration, waste at field use, and leakage from abandoned wells and coal mines are largely undocumented and assumed here to be of little economic value and therefore negligible.

We mapped the global distribution of natural gas production using production statistics [*U.N. Department of International Economic and Social Affairs*, 1986] and locations of major oil and gas wells [e.g., *Espenshade*, 1978; *Central Intelligence Agency*, 1978; 1985; *Seydlitz Weltatlas*, 1984]. As is expected, there is a high density of production sites in the Middle East, and in the Ob region of West Siberia. Some of the flaring sites were verified using a poster of nocturnal light intensities composited from satellite images from the Defense Meteorological Satellite Program [*Sullivan*, 1985].

Barns and Edmonds [1990] have documented the history of natural gas production since 1950. The vented and flared fraction shows large fluctuations: it was as high as 12% in the early 1970s and was at its minimum (~5%) in the early 1980s. Data on amounts of natural gas flared and vented [*U.S. Department of Energy*, 1986*a*, *b*] show a distinct geographic pattern. In 1984, venting and flaring was only 1% of marketed production in North America, 2% in Western Europe, 2% in Eastern Europe and the USSR, 11% in Asia and Australia, 18% in Central and South America, 40% in Africa, and was as high as 61% in the Middle East. Globally, venting and flaring was 3,533 billion cubic feet and corresponded to 5.7% of the marketable production in 1984.

To estimate the atmospheric methane from this source, it is necessary to determine the uncombusted fraction of methane that escapes to the atmosphere during flaring and venting at wells. *Darmstadter et al.* [1987] and *Barns and Edmonds* [1990] assumed that 20% of the flared/vented natural gas escapes directly to the atmosphere, thus yielding a methane source of ~15 Tg/yr. There are no direct measurements of this fraction and hence the contribution of this term to the global budget is highly uncertain.

The modeled atmospheric methane response to an assumed source strength of 50 Tg/yr (experiment GV) is shown in Figure 2*h*. Of note are the elevated concentrations of ~20 ppbv in the large fields in the River Ob Region of West Siberia and ~30 ppbv from the venting in the Middle East.

For GV(50) the simulated concentration is ~15 ppbv higher at the northern hemisphere NOAA/CMDL sites than at the southern hemisphere sites (Figure 3*b*). This north-south

difference is smaller than that caused by sources more proximate to the monitoring sites, for example, LF(50). Similarly, the seasonal cycles simulated at the sites for GV(50) are small compared to the observations (Figure 4*b*).

4.6. *Natural Gas Consumption*

With global annual natural gas consumption equivalent to ~1200 Tg CH_4/yr, transmission loss or pipeline leakage of natural gas may be a nonnegligible source of atmospheric methane. Direct estimation of these inadvertent losses of methane is difficult. Indirect limits may be obtained from discrepancies in billing, which include faulty meters, erroneous meter readings, theft and transmission losses. These discrepancies are reported as "unaccounted-for" natural gas [*U.S. Department of Energy,* 1986*b*] or as "line loss, etc." [*Statistics Canada*, 1986]. We estimated a loss rate of ~1% for Canada and 2.5% for the U.S.A. Applying this loss rate to the whole world would yield a global source strength of 10–36 Tg/yr.

Using our global data base on political units, human population densities and statistics on natural gas consumption for each country [*U.N. Department of International Economic and Social Affairs,* 1986] and each state of the U.S.A. [*U.S. Department of Energy,* 1986*b*] we mapped the global distribution of natural gas consumption by assuming that usage within a political unit is proportional to population density in that unit. Transmission loss of methane is assumed to be a globally uniform fraction of gas consumption. In experiment GL a basis source strength of 50 Tg was used.

The atmospheric methane response to GL(50) is shown in Figure 2*i*. The near-surface methane concentration is elevated by ~30 ppbv over Eastern U.S.A. and by ~40 ppbv over Central Europe where natural gas is in common use. The concentration is ~25 ppbv higher at middle latitudes in the northern hemisphere monitoring sites than at SPO (90°S) (Figure 3*b*). Because this source is widely distributed in North America, it gives the highest north-south gradient at the monitoring sites of all the aseasonal mid-latitude sources investigated.

4.7. *Coal*

Methane is the major component of coal gas, and is released to the atmosphere in the mining and processing of coal. We digitized, at 1°×1° resolution for the globe, the locations and approximate sizes of coal mines [*Espenshade,* 1978; *Central Intelligence Agency,* 1978; 1986; *Seydlitz Weltatlas*, 1984]. Country statistics on coal production [*U.N. Department of International Economic and Social Affairs,* 1986] were proportionately distributed among these mines. In 1984, approximately 2.9×10^{12} kg of hard coal equivalent were produced. (By definition, 1 kg hard coal equivalent has a gross caloric value of 7000 kcal, close to the maximum value attainable when burned under ideal conditions.) Coal gas is ~95% methane. While the amount of coal gas increases with the depth of coal deposits [*Darmstadter et al.*, 1987], no attempt was made to distinguish among anthracite, bituminous, brown and other types of coal, as such information was not consistently available for most of the coal-producing countries. With ~15 L of coal gas per kilogram of coal, there were ~30 Tg CH_4 in coal produced in 1984. *Barns and Edmonds* [1990] estimated 25 Tg/yr. To obtain the methane emission pattern, we assumed that coal was processed in the vicinity of the mines, i.e., the methane emission pattern was the same as the mining pattern. As with the other sources, an arbitrary source strength of 50 Tg was used in the three-dimensional simulations.

Figure 2*j* shows the near-surface methane concentrations from the CL(50) source are elevated by ~30 ppbv over the coal mining regions of the Eastern U.S.A. (West Virginia, Kentucky, and Pennsylvania) and Europe (Poland and West Germany). Elevated concentrations of >20 ppbv are also found over the River Ob region in the state of Russia and over China. The north-south gradient (Figure 3*b*) and peak-trough amplitudes (Figure 4*b*) show patterns similar to the other mid-latitude sources.

4.8. *Biomass Burning*

Crutzen and Andreae [1990] estimate that biomass burning in the tropics releases 1800 to 4700 Tg C annually, with 11–53 Tg as methane. *Craig et al.* [1988] have used the $^{13}C/^{12}C$ ratio of atmospheric methane to infer that the methane flux from biomass burning is 52 Tg/yr. *Cicerone and Oremland* [1988] assumed this source to be 55 Tg/yr. The geographic information is scanty. We mapped the distribution of CO_2 release due to land use modification in the tropics [*Houghton et al.*, 1987] and assumed that methane release due to biomass burning is proportional to CO_2 release [*Crutzen et al.*, 1979; *Crutzen and Andreae,* 1990]. The CO_2 release pattern is similar to that compiled by *Detweiler and Hall* [1988]. The use of a single CH_4/CO_2 proportionality constant for the whole globe is not strictly valid, as the deforestation CO_2 source is not only direct inputs from fires, but also includes the net release of CO_2 due to oxidation of soil carbon over regrowth of vegetation. Also, in South and Southeast Asia, where commercial logging rather than slash and burn agriculture may be an important mode of deforestation, this assumption may overestimate the methane source due to biomass burning. Furthermore, CH_4/CO_2 ratios from biomass burning are found to depend on vegetation and fire characteristics [e.g., *Cofer et al.*, 1990]. Nevertheless, the methane source mapped here is similar to that compiled independently by *Hao et al.* [1990] who made similar assumptions. Experiment BB assumes that the biomass burning release is during the dry season, determined as the months when precipitation is less than potential evaporation (cf. section 4.1).

The annual mean methane distribution near the surface resulting from the BB(50) source is shown in Figure 2*k*. Concentration elevations of >10 ppbv are simulated over Brazil, tropical Africa, and Southeast Asia. The north-south gradient at the NOAA/CMDL sites shows a maximum of 9 ppbv at CHR (2°N) in the tropics relative to SPO (90°S) (Figure 3*c*). The peak-trough amplitude also peaks at ~6 ppbv at CHR (2°N) (Figure 4*c*).

4.9. *Termites*

There is a wide range of estimates (0–200 Tg) for the contribution of this source to the global budget [*Zimmerman et al.*, 1982, 1984; *Zimmerman and Greenberg,* 1983; *Rasmussen and Khalil,* 1983*a*, *b*; *Seiler et al.*, 1984; *Fraser et al.*, 1986*b*]. This has been discussed by *Cicerone and Oremland* [1988].

Termite habitats are generally located in tropical grasslands and forests [*Zimmerman et al.*, 1982; *Fraser et al.*, 1986*b*]. We mapped the potential habitats of termites using the global vegetation data base of *Matthews* [1983]. Assuming an aseasonal source of 50 Tg/yr, we distributed the emission among ecosystems according to the tabulations of *Zimmerman et al.* [1982, 1983] and *Fraser et al.* [1986*b*], with 41% emanating

from savannas and 35% from tropical forests. Because the assumed habitat is widely distributed in the tropics and subtropics over an area of $\sim 100 \times 10^{12}$ m^2, the local methane flux is weak, < 0.002 g $CH_4/m^2/d$ for TM(50). The resulting atmospheric distribution for experiment TM(50) (Figure 2*f*) shows maximum elevations of 6–8 ppbv above the global mean in the tropical regions. The effect on mid-latitude concentrations is small. The peak concentration in the tropics is 6 ppbv above that of SPO (Figure 3*c*). Correspondingly, the simulated peak-trough amplitudes at the monitoring sites are small and due entirely to variations in atmospheric transport (Figure 4*c*).

4.10. *Hydrates/Clathrates*

The potential release of methane from hydrates/clathrates is highly uncertain. While methane hydrates are known or inferred to be found on the continental shelf at all latitudes [*Kvenvolden*, 1988], it is generally hypothesized that those hydrates located in the Arctic, in particular the offshore permafrost, are subject to destabilization due to climate warming [*Bell*, 1983; *Revelle*, 1983; *Kvenvolden*, 1988].

To test the atmospheric methane signature from such a source, we simulated the atmospheric methane distribution in response to two hypothetical methane sources in the Arctic. Experiment HV distributed 10 Tg in the coastal areas of the Soviet Arctic, from 90°E to 140°E and from 72°N to 80°N. Experiment HZ distributed 10 Tg in a zonally uniform belt extending from 80°N to 88°N. The annual mean concentration variations near the surface are shown in Figures 2*m* and 2*n*.

ALT (82°N) is elevated ~38 ppbv above SPO (90°S) in HZ(10) and by ~13 ppbv in HV(10) (Figure 3*d*). The largest concentration is found in the Arctic: ϕ(ALT) – ϕ(BRW) is 16 ppbv in HZ(10) and is ~2 ppbv in HV(10). Farther south, near CBA (55°N) on the south coast of Alaska, the concentrations are similar in the two cases: the elevation relative to SPO (90°S) is ~8 ppbv at CBA (55°N) and ~5 ppbv at KUM (20°N). The annual cycle at the high-latitude sites reflects the spring breakdown of the polar vortex: the concentration peaks in April at ALT (82°N), with a peak-trough amplitude of ~24 ppbv in HZ(10) and ~10 ppbv in HV(10).

4.11. *Chemical Destruction*

Methane is destroyed predominantly in the troposphere by reaction with the hydroxyl radical OH. The rate coefficient k_c for the reaction,

$$CH_4 + OH \Rightarrow CH_3 + H_2O \qquad (3)$$

is generally taken to be $k_c = 2.3 \times 10^{-12} \exp(-1700/T)$ cm^3 s^{-1} [*DeMore et al.*, 1987]; T is temperature (in Kelvin). The OH radical is extremely short-lived in the troposphere, reacting primarily with CO or CH_4 on time scales of 10 s or less. Concentrations of OH are predicted to vary as a function of the local abundances of O_3, H_2O, CO, CH_4, NO_x(=NO+NO_2) and temperature; OH levels also vary diurnally. We lack the direct observations of OH that would allow us to integrate the global methane loss. One approach in calculating chemical budgets has been to apply a theoretical model for the tropospheric photochemistry and to test the resulting OH fields using a well observed species with known sources, such as CH_3CCl_3 [e.g., *Logan et al.*, 1981; *Rasmussen and Khalil*, 1984*b*; *Prinn et al.*, 1987].

The global distributions of OH used here were taken from *Spivakovsky et al.* [1990*a*, *b*]. They calculated the three-dimensional global distribution of OH every 5 days over a year as a function of sunlight and trace gas concentrations. The local independent variables needed to compute OH were taken from the parent GCM (5-day averages of pressure, temperature, water vapor, and cloud cover), and from observed climatologies for CO, O_3, CH_4, NO_x, water vapor above 500 mbar, and the overhead ozone column. The data base is insufficient to define four-dimensional fields for these species, so the model relied on monthly mean concentrations, and used zonal average distributions with smooth variations over latitude, altitude, and season. The exceptions were CO and NO_x, for which higher values were adopted in the continental boundary layer than in the marine boundary layer, and ozone, for which higher values were used over the tropical continents than over the oceans.

The four-dimensional distribution of OH implies a lifetime for CH_3CCl_3 of 5.5 years, somewhat shorter than that derived from the observations, 6.3 (+1.2, –0.9) years (1σ uncertainty) [*Prinn et al.*, 1987] Consequently model levels of OH may be too high by about 13%, assuming that global emissions estimates and the absolute calibration of the CH_3CCl_3 measurements are correct. The reader is referred to *Spivakovsky et al.* [1990*b*] for further discussion of constraints on OH imposed by the data for CH_3CCl_3, and for details of the OH calculation. The numerical method used for parameterization of the chemistry is described in the work by *Spivakovsky et al.* [1990*a*].

We used the three-dimensional distributions of the 5-day averages of OH and the temperature for each model gridbox to calculate the loss rate of methane in the model:

$$\text{Loss} = k_c\ [OH]\ [CH_4] \qquad (4)$$

The OH fields were multiplied by 0.85 to be consistent with a CH_3CCl_3 lifetime of 6.3 years. The reduction of 15% is within the uncertainty range (0.75±0.25) quoted by *Spivakovsky et al.* [1990*a*].

The calculation of the photochemical signal in methane is based on losses evaluated for a fixed distribution (1700 ppbv in the northern hemisphere and 1600 ppbv in the southern hemisphere). The model calculation was initialized with zero methane concentration in the atmosphere and integrated for 4 years until a steady pattern of chemically driven variations developed. The tropospheric losses are countered by a tropospherically uniform fill of methane that is equal to the annual globally integrated sink. In other words, at the end of each year's cycle the globally averaged methane abundance is zero.

For the case of multiple sources, the concept of separate simulations for each source followed by a linear recomposition of the signal at an observing site is mathematically rigorous. In the case of chemical destruction in the atmosphere, methane loss is linearly proportional to its concentration and hence cannot be strictly separated from its local abundance. The errors in the approach adopted here are limited by the variations in methane about the assumed value. Within each hemisphere, average latitudinal variations in methane are observed to be less than the interhemispheric gradient of 6% (see Figure 1). Similarly, observed seasonal variations over the year at remote sites in mid-latitudes are at most 3% (50 ppbv). Near and above source regions, however, the abundance may be elevated by 20% (330 ppbv) or more, but the fraction of the atmosphere (and also the chemical loss) in such regions is small at the global scale. Any such errors will be further damped by

TABLE 5. Distribution of Annually Averaged Chemical Loss Rate for Methane in the Atmosphere, Expressed as a Percentage of the Global Total Loss

Latitude	Surface - 800 mbar	800 - 600 mbar	600 - 400 mbar	400 - 200 mbar	200 - 0 mbar	Column
80°N-90°N	0.0	0.0	0.0	0.0	0.0	0.2
70°N-80°N	0.2	0.2	0.1	0.0	0.1	0.6
60°N-70°N	0.5	0.4	0.2	0.1	0.2	1.4
50°N-60°N	0.8	0.8	0.4	0.1	0.3	2.4
40°N-50°N	1.4	1.4	0.7	0.2	0.4	4.2
30°N-40°N	2.4	2.4	1.4	0.4	0.5	7.1
20°N-30°N	3.4	3.6	2.2	0.6	0.6	10.4
10°N-20°N	4.4	4.4	2.7	0.8	0.7	13.0
0°-10°N	4.7	4.9	3.1	0.9	0.8	14.4
10°S-0°	4.2	4.5	3.0	1.0	0.7	13.5
20°S-10°S	3.8	3.9	2.7	0.9	0.7	11.9
30°S-20°S	3.3	3.3	2.1	0.7	0.6	10.0
40°S-30°S	1.9	1.8	1.2	0.4	0.5	5.8
50°S-40°S	0.7	0.8	0.6	0.2	0.4	2.7
60°S-50°S	0.3	0.4	0.3	0.1	0.3	1.4
70°S-60°S	0.1	0.2	0.1	0.0	0.2	0.8
80°S-70°S	0.0	0.1	0.1	0.0	0.1	0.3
90°S-80°S	0.0	0.0	0.0	0.0	0.0	0.1
Global	32.0	33.3	21.0	6.4	7.3	100.0

Global loss is 450 Tg/yr, corresponding to a lifetime of 10.1 yr. Unit is percent. Due to rounding, values in columns and rows may not total exactly.

the inherent feedbacks in the OH–CH_4–CO system [*Sze*, 1977] where high values of CH_4 and CO depress OH concentrations. Thus we estimate that errors in the total budget or in the latitudinal and seasonal patterns of CH_4 presented here under the assumption of fixed losses are less than 5% of the calculated signal (for example, the seasonal amplitude at high N and S latitudes is 40±2 ppbv).

The distribution of chemical loss of CH_4 is summarized in Table 5 for a global sink strength of 450 Tg CH_4/yr, corresponding to a scaling factor of 0.85 for the OH field. Unlike many of the sources which are highly localized at the surface, methane loss occurs throughout the entire atmosphere. The destruction rate is highest in the lower tropical troposphere: OH concentrations peak where high values of water vapor and temperature coincide with the brightest intensity of sunlight. Stratospheric losses of methane are of secondary importance and contribute about 7% to the total sink.

New laboratory measurements of the rate coefficient k_c [*Vaghjiani and Ravishankara*, 1991] show it to be slower than previously adopted [*DeMore et al.*, 1987]. If we use the new rate and scale it to a CH_3CCl_3 lifetime of 6.3 years in the manner verified by *Prather and Spivakovsky* [1990], we get a lifetime of 11.3 years with an uncertainty of ±10% associated with determination of k_c alone. (Larger uncertainties apply to the CH_3CCl_3 lifetime and rate coefficient.) The corresponding range in CH_4 loss is 365 to 445 Tg CH_4/yr.

Figure 2*o* shows the annually averaged near-surface methane distribution resulting from chemical destruction alone (experiment CH(–450)). The concentration in the tropics is depressed on average ~30 ppbv below the global mean, with the depression slightly larger over land areas. The maximum latitudinal gradient (equator to pole), for example, CHR (2°N) to SPO (90°S), is ~35 ppbv (Figure 3*e*). The peak-trough amplitude of the seasonal cycle at mid-latitudes is comparable to the magnitude of the latitudinal gradient (~40 ppbv). The rate of chemical destruction maximizes in late summer, and is least in late winter. Seasonal cycles persist into the subtropics and disappear near the equator.

4.12. *Soil Absorption*

Uptake of methane by dry soils has been observed in a few limited studies (e.g., *Harriss et al.*, 1982; *Keller et al.*, 1983, 1990; *Steudler et al.*, 1989; *King et al.*, 1989; *Whalen and Reeburgh*, 1990*b*]. Recently, *Born et al.* [1990] found that soil absorption of methane is directly related to soil texture, and using soil-vegetation associations, arrived at ranges of methane absorption rates for seven vegetation groups and global estimates of 6–58 Tg/yr. Temperate and boreal forests, with relatively high absorption rates (0.09–1.3 g CH_4/m^2/yr) and large areal extents, account for 35–50% of the global sink.

We distributed the *Born et al.* [1990] flux rates using the *Matthews* [1983] vegetation data base. Seasonality of soil absorption was not included in the simulation since microbial activity appears to be controlled mainly by gas transport in the soil rather than by soil temperature [*Born et al.*, 1990]. Model experiment SA was run with an aseasonal source with basis strength of 50 Tg/yr.

The atmospheric methane response is shown in Figures 2*p*, 3*b* and 4*b*, where for convenience the response was plotted with a sign change for direct comparison with the mid-latitude aseasonal sources. Concentrations are depressed by ~18 and ~28 ppbv below the global mean over boreal forests of North America and Siberia. At the monitoring sites the largest north-south gradient, ~26 ppbv, is found between STM (66°N) and SPO (90°S). The largest seasonal amplitude is again found at high latitudes due to the seasonality of the circulation.

4.13. *Other Sources and Sinks*

We have not carried out three-dimensional simulations for scenarios of several methane sources and sinks that are extremely poorly known or whose contribution to geographic

and intra-annual variations may be very small. These sources/sinks include (1) oceans and lakes [*Ehhalt*, 1974], (2) release of methane from asphalt [*Sackett and Barber*, 1988; *Tyler et al.*, 1990], and (3) leakage of methane from biogas generators [*Khalil et al.*, 1990]. While these sources/sinks may be included in the budget, we assumed that they contribute little to the seasonal and geographic variations of methane in the atmosphere.

5. Constraints on the Global Methane Budget

A global budget of atmospheric methane can be constructed, as a first approximation, as a linear combination of the sources and sinks.

$$M^{n+1} = M^n + \sum_j S_j - k_{OH} * M^n - k_{soil} * M^n \quad (5)$$

Equation (5) states that the difference between the mass M of methane in the atmosphere between year n+1 and year n is the algebraic sum of the annual sources S_j and sinks. The sinks included are OH destruction and soil absorption and are given by the destruction rate k_{OH} and absorption rate k_{soil}, respectively, multiplied by the mass of methane in the atmosphere.

Isotopic composition of the sources and sinks and of atmospheric methane provide additional constraints on the global budget [*Stevens and Engelkemeir*, 1988; *Cicerone and Oremland*, 1988; *Wahlen et al.*, 1989]. The mass balance for $^{13}CH_4$ can be similarly expressed as

$$\begin{aligned} R^{n+1} * M^{n+1} = {} & R^n * M^n + \sum_j R_j * S_j \\ & - (k_{13}/k_{12})_{OH} * k_{OH} * R^n * M^n \\ & - (k_{13}/k_{12})_{soil} * k_{soil} * R^n * M^n \end{aligned} \quad (6)$$

where

$$R = \frac{(^{13}C/^{12}C)_{sample}}{(^{13}C/^{12}C)_{standard}} = \frac{\delta^{13}C_{sample}}{1000} + 1 .$$

In this study we constructed global methane budget scenarios and tested their ability to reproduce the observed geographic observations. To reduce the degrees of freedom in the construction of the scenarios, we maintained several conditions imposed by the concentration and isotope data, some of which have been discussed by *Cicerone and Oremland* [1988]:

Condition 1 (C1): The current rate of increase, $M^{n+1} - M^n$, is approximately 40 Tg/yr.

Condition 2 (C2): Two sink strengths for OH destruction were tested: scenarios 1-4 used $k_{OH} * M^n = 500$ Tg/yr while scenarios 5-7 used $k_{OH} * M^n = 450$ Tg/yr.

Condition 3 (C3): The soil sink $k_{soil} * M^n$ was varied between 0 and 60 Tg/yr to optimize the fit between the observed and modeled distributions. The limits were given by *Born et al.* [1990].

Condition 4 (C4): We tested fossil source fractions of −27, −20, and −16% in the different budget scenarios. These fractions represent the range of estimates based on the $^{14}CH_4$ data. We assumed the fossil fraction comprised emissions from coal mining, natural gas venting and leakage, and clathrate destabilization.

Condition 5 (C5): We used a global annually averaged $\delta^{13}C$ of atmospheric methane of −47.2±0.1 °/oo [*Quay et al.*, 1991]. This value differs by ~0.5 °/oo or larger among different investigators. Because this uncertainty encompasses the trend in $^{13}CH_4$ reported by *Stevens* [1988] and *Stevens and Englekemeir* [1989] for this period, we assumed that $R^{n+1} \approx R^n$.

Condition 6 (C6): We used kinetic fractionation ratios $(k_{13}/k_{12})_{OH} = 0.9946 \pm 0.0009$, and $(k_{13}/k_{12})_{soil} = 0.979$ based on recent measurements by *Cantrell et al.* [1990] and *King et al.* [1989], respectively. In this way, the weighted average of the $\delta^{13}C$ of the sources is calculated using Equation (6), and would range between −52.8 °/oo and −54.3 °/oo for 0–10% soils contribution to the total sink strength. Because the soil sink is expected to be small, uncertainties in $(k_{13}/k_{12})_{soil}$ do not have a large impact on the results.

Condition 7 (C7): The range of isotopic values measured for each of the sources is given in Table 3. R_j for each source was selected from within the measured range to satisfy Equation (6).

Seven candidate budget scenarios are listed in Table 6. These scenarios meet the constraints above on the mass balance of $^{12}CH_4$, $^{13}CH_4$ and $^{14}CH_4$. The animal source was fixed at 80 Tg/yr, as this is perhaps one of the better known sources in the budget [*Crutzen et al.*, 1986]. The acceptance of candidate budget scenarios was based on the ability of the scenario to match, in addition, observed geographic and temporal features in the atmosphere: condition 8 (C8): the annual mean north-south gradient of atmospheric methane measured at the NOAA/CMDL network; and condition 9 (C9): the methane seasonal cycle at each of the observing stations.

6. Analysis of Budget Scenarios

Seven budget scenarios are constructed according to the constraints C1–C7 outlined above (Table 6). Budget scenario 1 is that given by *Cicerone and Oremland* [1988]. Scenarios 2-4 used a chemical destruction rate of 500 Tg/yr, while scenarios 5-7 used a destruction rate of 450 Tg/yr. For each chemical destruction rate, fossil fractions comprising ~27, 20 and 16% of global sources were investigated. The total atmospheric methane distribution corresponding to each of the budget scenarios was calculated as the linear combination of the responses to the individual source/sink functions. In this section, we apply constraints 8 and 9 and test whether the modeled atmospheric distribution matches that observed.

In scenario 1 the wetland source is W1, with a global strength of 110 Tg, and seasonality of emission given by *Matthews and Fung* [1987]. A tundra emission of 5 Tg (WT) was included. As can be seen in Figure 5, the simulated pole-to-pole difference in concentration is ~200 ppbv, an overestimate of ~60 ppbv. Figure 6 shows the comparison of the modeled and observed seasonal cycles at a few sites. The left panels show the modeled seasonal cycle $\xi(STN,t)$ for each source/sink with the strength specified in the budget scenario. These individual cycles are summed to form the total seasonal cycle modeled for this scenario, which is compared with the observed cycle in the right panel. The modeled seasonal cycle agrees well with the observed cycles at SPO and other middle- to high-latitude stations in the southern hemisphere: the seasonal cycle is dominated by that of chemical destruction which maximizes in summer (cf. Table 5). At MLO (20°N) the interaction between the cycles of chemical destruction and seasonal emissions from wetlands and rice paddies results in a complex annual cycle which resembles that observed: a broad peak of ~8 ppbv above the annual mean from January to March, a trough of ~15 ppbv in July/August as a result of the seasonality in chemical destruction, and a second peak of ~14 ppbv in November dominated by biological emissions in the summer.

TABLE 6. Methane budget scenarios

Source/Sink	Scenario 1		2		3		4		5		6		7	
Animals	80	(-60)	80	(-68)	80	(-62)	80	(-59)	80	(-68)	80	(-70)	80	(-60)
Wetlands														
bogs/tundra	80	(-60)	35	(-65)	35	(-60)	35	(-60)	35	(-65)	35	(-65)	35	(-61)
swamps/alluvial	35	(-60)	70	(-60)	75	(-60)	60	(-60)	55	(-60)	45	(-65)	80	(-61)
Rice	110	(-63)	100	(-63)	110	(-63)	100	(-63)	100	(-65)	50	(-65)	100	(-62)
Landfills	40	(-50)	20	(-53)	20	(-50)	15	(-53)	20	(-53)	40	(-53)	40	(-51)
Natural gas vents	20	(-38)	80	(-42)	65	(-40)	20	(-38)	80	(-38)	25	(-42)	10	(-41)
Natural gas leaks	25	(-38)	40	(-42)	20	(-38)	25	(-38)	15	(-38)	35	(-42)	30	(-41)
Coal mining	35	(-38)	35	(-42)	25	(-38)	35	(-35)	40	(-38)	35	(-42)	35	(-41)
Biomass burning	55	(-25)	60	(-27)	50	(-27)	55	(-24)	50	(-25)	100	(-28)	55	(-25)
Termites	40	(-60)	40	(-68)	40	(-60)	100	(-59)	15	(-68)	40	(-68)	20	(-60)
Methane hydrates	5	(-65)	5	(-65)	5	(-65)	5	(-65)	0	(-65)	5	(-65)	5	(-65)
Oceans and freshwaters	15	(-40)	15	(-40)	15	(-40)	10	(-40)	10	(-40)	10	(-40)	10	(-40)
Total sources	540	(-52.5)	580	(-53.5)	540	(-52.4)	540	(-52.6)	500	(-52.7)	500	(-52.8)	500	(-52.9)
% fossil	16		28		21		16		27		20		16	
% wetlands	21		18		20		18		18		16		23	
% rice	20		17		20		19		20		10		20	
% animals + termites	22		21		22		33		19		24		20	
% biomass burning	10		10		10		10		10		20		11	
Chemical destruction	500		500		500		500		450		450		450	
Soil absorption	0		40		0		0		10		10		10	
Total sinks*	500	(-52.3)	540	(-53.4)	500	(-52.3)	500	(-52.3)	460	(-52.7)	460	(-52.7)	460	(-52.7)

Annual source and sink strengths are in Tg CH_4/yr. Numbers in parenthesis denote $\delta^{13}C$ of sources or sinks in per mil.
* A $\delta^{13}C$ value of -47.2 °/oo for atmospheric methane, isotopic fractionation effects of 0.9946 for oxidation by OH and of 0.979 for soil absorption were used in the calculation.

The agreement between the observed and modeled annual cycles deteriorates northward of MLO (20°N). At BRW (71°N) the observed and modeled cycles are completely out of phase. It is clear from Figure 6 that the modeled wetland source (W1) yields a very large annual cycle at high latitudes with peak concentrations in the summer. This large annual cycle is due to the emission rate (0.2 g/m^2/d) assumed for the entire emission season from forested and nonforested bogs. Such a high emission rate may not be representative, as suggested by the results from ABLE IIIA and *Whalen and Reeburgh* [1988].

Common to scenarios 2-7 is the use of wetland emissions from experiments WB, WT, and WS. Emissions from high-latitude bogs in these scenarios, WB(30) + WT(5), represent extrapolation from recent flux measurements and are smaller by a factor of 2 compared to that in scenario 1. The remaining sources in each of the scenarios were then adjusted until mass constraint (Equation (5)) was satisfied and until the $\delta^{13}C$ of the combined sources was within ±0.3 °/oo of the $\delta^{13}C$ of the combined sinks (Equation (6)).

The atmospheric concentrations simulated with scenarios 2-7 compare well with the observations, both in terms of the annual mean north-south gradients (Figure 5) and the seasonal cycles at the stations. Figure 7 shows the simulated and observed annual cycle at each of the observing sites for scenario 7. The annual cycles simulated in the other budget scenarios are very similar. The composition of the modeled annual cycles (left panels) show clearly the dominance of chemical destruction in the seasonal variations of atmospheric methane in the southern hemisphere, where seasonal signals from both wetlands and rice fields are diluted. In the northern hemisphere, reasonable agreement between modeled and observed cycles was found at all the stations. Compared to scenario 1, the improved agreement with the observations at CBA (55°N) and BRW (71°N) comes from the improved description of seasonal emissions from high-latitude bogs.

It is clear that while six budget scenarios presented above satisfy all the available constraints, they do not represent a comprehensive set of budget scenarios. For example, because the $\delta^{13}C$'s of methane from tropical swamps and from rice fields are similar, all the constraints could have been met equally with a shift of, say, 20 Tg from the rice source to the swamp source. In Table 6, individual source terms range by a factor of 2 among the scenarios presented. This range is comparable to that presented by *Ehhalt* [1974], *Cicerone and Oremland* [1988] and others, who used mainly constraints C1–C7. It is wrong, however, to conclude that geographic and temporal variations of methane in the atmosphere (constraints C8 and C9) present no additional constraints on the global methane budget. By comparing the fluxes of methane directly measured or estimated with the average fluxes implied by each of the sources in scenarios 2-7, we were further able to eliminate scenarios 2-6 as likely global methane budgets. In the following we describe how we arrived at scenario 7 as the preferred budget scenario.

To examine the geographic constraints on methane sources and sinks, it is easiest to start with regions with a single source/sink, or regions with distinctive atmospheric signatures. Such a region is the mid-latitudes in the southern hemisphere

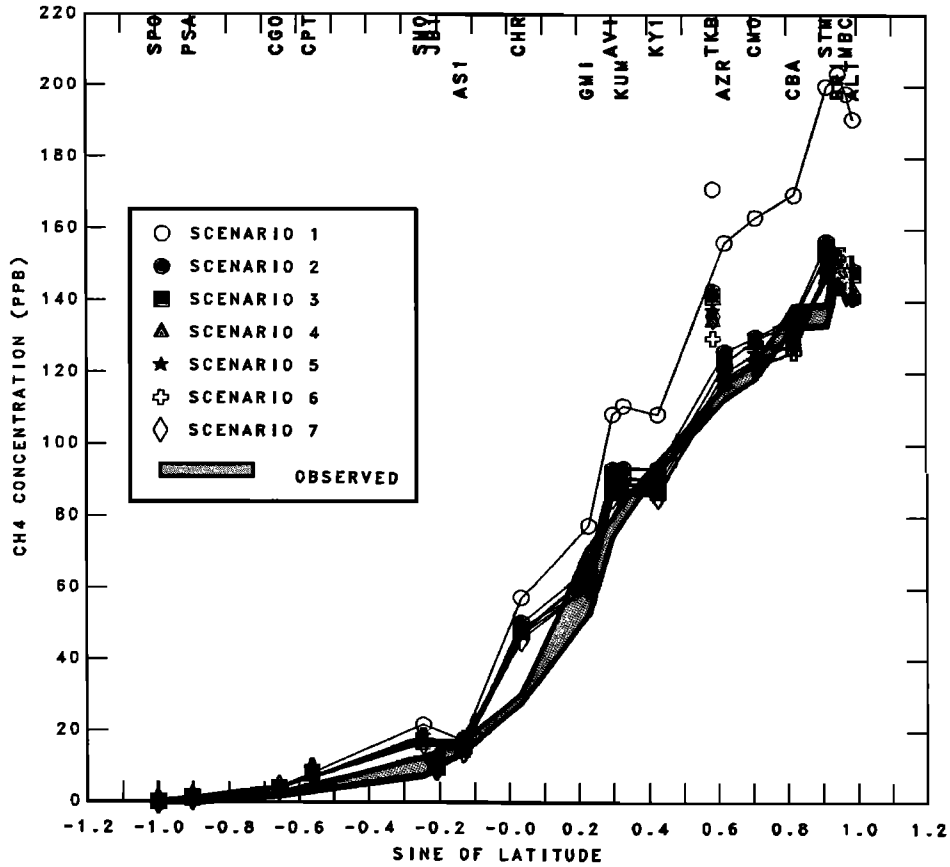

Fig. 5. Comparison of the observed annual mean methane concentrations at the observing sites with those simulated for global budget scenarios 1-7 (Table 6). All concentrations are defined relative to the concentration at the South Pole, ϕ(STN) - ϕ(SPO). The thick solid lines and shaded region denote $\pm 1\sigma$ range of the NOAA/CMDL data in the marine boundary layer. The thin solid lines connect values modeled at the NOAA/CMDL sites, leaving modeled values at CPT, JB1, and TKB off the line.

where chemical destruction is the only source/sink term of significance. Successful simulation of seasonal methane variations at CGO (41°S) and CPT (34°S) here further supports the four-dimensional OH fields derived by *Spivakovsky et al.* [1990*b*] and the rate coefficient k_c used. We note that a 10% variation in the annual chemical destruction, between 500 and 450 Tg/yr, cannot be distinguished with confidence within uncertainties in transport characteristics of the GCM and the resolution of the tracer model.

From the southern hemisphere we proceeded to polar and high latitudes in the northern hemisphere, where sources are few and their atmospheric methane signatures are distinct. The only hypothesized methane source at polar latitudes in the northern hemisphere is from destabilization of hydrates/clathrates. The locations where this source is active currently are not known. On the basis of the fact that the observed annual mean concentration at ALT (82°N) is lower than that at BRW (71°N), we ruled out a zonally active source HZ >5 Tg/yr, since it would elevate ϕ(ALT) relative to ϕ(BRW) by at least 10 ppbv. A source active only in regions far away from the monitoring sites, for example, in the Soviet Arctic (Experiment HV, cf. Figure 3*d*), cannot be ruled out by the available observations.

There are four known seasonal sources and sinks: chemical destruction, natural wetlands, rice cultivation, and biomass burning. At BRW (71°N) and other high-latitude stations in the northern hemisphere the model shows that seasonal CH_4 variations are caused by chemical destruction and by high-latitude bogs, the signals from tropical and subtropical sources being too diluted to have an impact on the seasonal cycle at high latitudes. If the seasonal cycle due to OH destruction is assumed to be correct, then an emission of 35 Tg/yr from the wetlands and tundra north of 50°N is tolerated by the atmospheric observations. A larger emission, such as that estimated by *Matthews and Fung* [1987] and used in scenario 1 (Figure 6) would exaggerate the summer peak. The emission is assumed to occur during the summer months when the soils are not frozen. A longer emission period could also contribute to a larger annual emission but is not supported by the very low winter fluxes measured by *Whalen and Reeburgh* [1988]. We have not included seasonality of the source/sink terms other than the four mentioned above as they are not well known and not likely to have significant impact on the high-latitude seasonal cycle of atmospheric methane. The only exception may be the soil sink, whose seasonal cycle (absorption in the dry season) would be in phase with the wetland cycle (emission in the wet season). If a significant soil sink cycle is included in the analysis, contribution of the wetland source would have to be further reduced to match the observed seasonal cycle at BRW (71°N).

Methane sources in mid-latitudes in the northern hemisphere are mainly associated with anthropogenic activity and are aseasonal. We have presented six northern hemisphere mid-latitude sources and sinks: animals, landfills, natural gas venting,

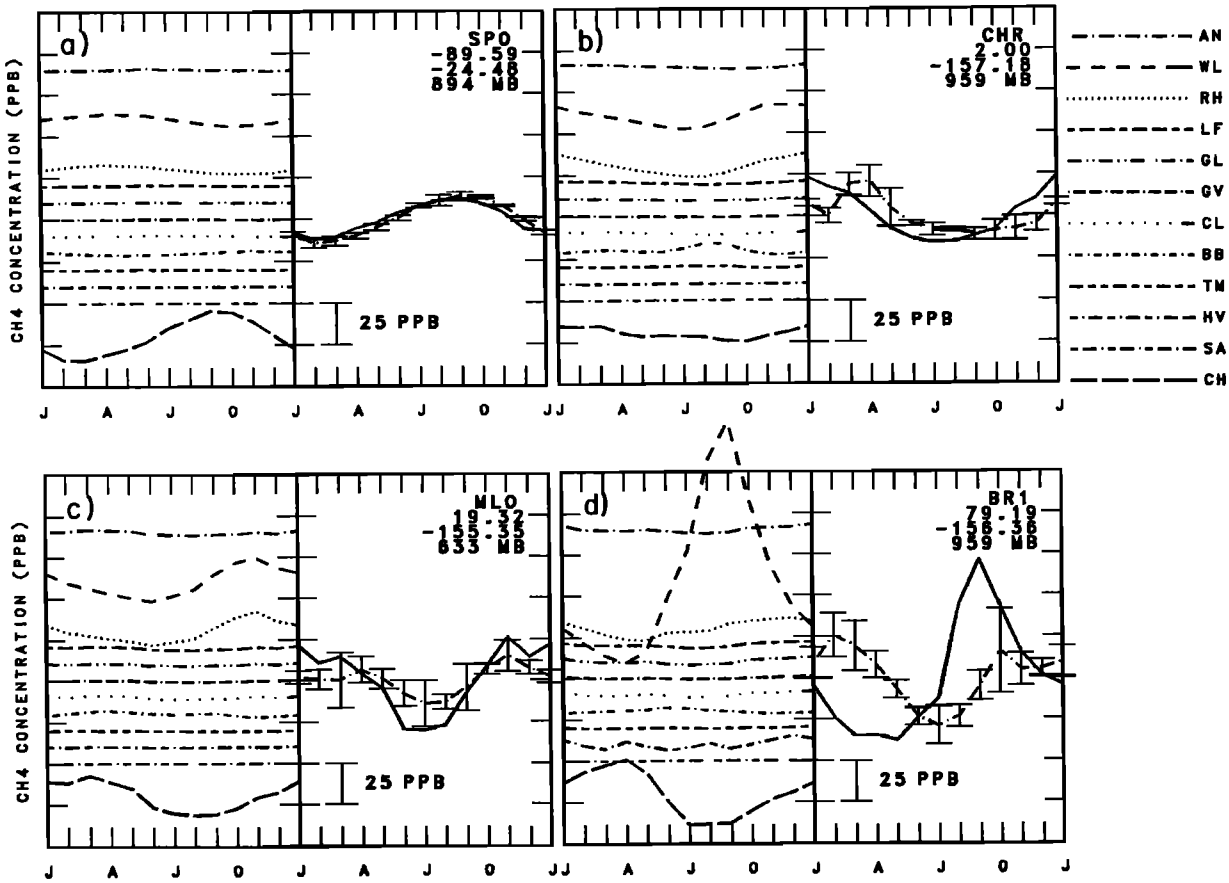

Fig. 6. Comparison of the observed seasonal cycle of atmospheric methane at a few sites with those modeled using budget scenario 1. The sites are (*a*) SPO (90°S), (*b*) CHR (2°N), (*c*) MLO (20°N), and (*d*) BRW (71°N). The left panels show the modeled atmospheric methane response to each of the source/sink terms in scenario 1. The lines are displaced along the ordinate to facilitate display. In the right panels the total modeled response (solid line) is the sum of the individual responses shown in the left panels. The mean (dashed lines) and one standard deviation are shown for the observed seasonal cycles. WL is the sum of the wetlands and tundra terms.

transmission loss, coal mining, and soil absorption. These sources and sinks have different longitudinal distributions. Hence, even if their source strengths were equal, they would produce north-south concentration profiles with similar shapes but different magnitudes at the monitoring sites (cf. Figure 3*b*). The north-south profile of the annual mean atmospheric methane concentration alone thus presents some, but not a unique, constraint on these mid-latitude sources.

Together with the ratio of $^{14}C/^{12}C$ in atmospheric methane, the north-south concentration profile places important limits on the mid-latitude sources. For a given fraction of fossil sources or a given total emission from these sources the partitioning among coal mining, natural gas venting and transmission loss can be adjusted to match the north-south gradient in atmospheric methane. For example, in scenario 6, where a total fossil source of 100 Tg/yr is tested, a shift of 10 Tg from venting sources (dominating in the USSR and Middle East) to transmission losses or coal mining (dominating in the U.S.A. and Western Europe) would exaggerate the north-south gradient at the monitoring sites located mainly in the Pacific Ocean. The partitioning among the three terms is of course not unique, and is affected by the uncertainties in the landfill and animal sources as well as in the soil sink.

In scenarios 2 and 5 the fossil fraction is 27%. In order to match the north-south methane gradient at the monitoring sites, 80 Tg of the fossil sources are required to come from locations remote from the monitoring sites, i.e., from the natural gas venting source. Statistics presented in section 4.5 on natural gas production give a methane source of 15 Tg/yr if 20% of the natural gas vented and flared at production sites escapes to the atmosphere as methane. Thus 75 Tg/yr is the absolute but unlikely upper bound on methane emissions from this source. We consider a fossil fraction of 27% highly improbable unless inadvertent and unaccounted-for natural gas escaping at wells and refineries comprises a significant term in the global methane budget, or unless there is a large clathrate source remote from the monitoring sites, such as in the Soviet Arctic. We hence reject scenarios 2, 3, and 5, as the vented component would comprise over 100% of the natural gas flared and vented at the wells. Similarly, scenario 6, with a vented fraction of 33%, is considered unlikely, although there are no data to eliminate it definitively. The magnitude of the fossil sources inferred here in scenarios 4 and 7 (16% of the global source strength) do not disagree with the direct estimates of *Barns and Edmonds* [1990].

It remains to seek constraints on tropical sources (swamps, termites, biomass burning, and rice cultivation). Tropical sources have little impact on the north-south gradient recorded at the current network (cf. Figure 3*c*). Also, while their emissions may be seasonal, the majority of monitoring sites are too distant to record their impact. Hence one constraint on their total strength is the residual in the global budget. Table

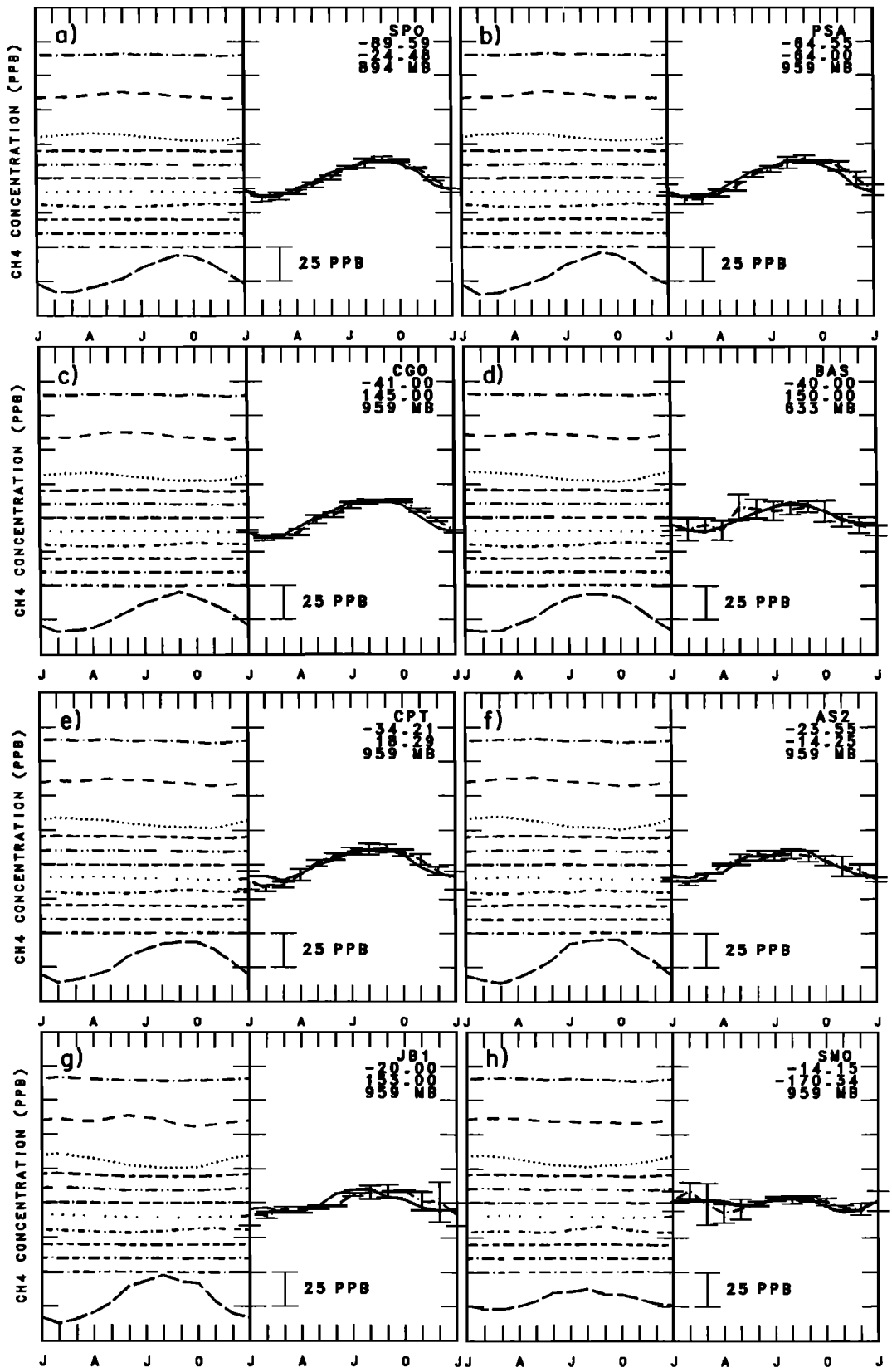

Fig. 7. Comparison of the observed seasonal cycle of atmospheric methane at all the observing sites with those modeled using scenario 7. Refer to Figure 6 for an explanation of the scales.

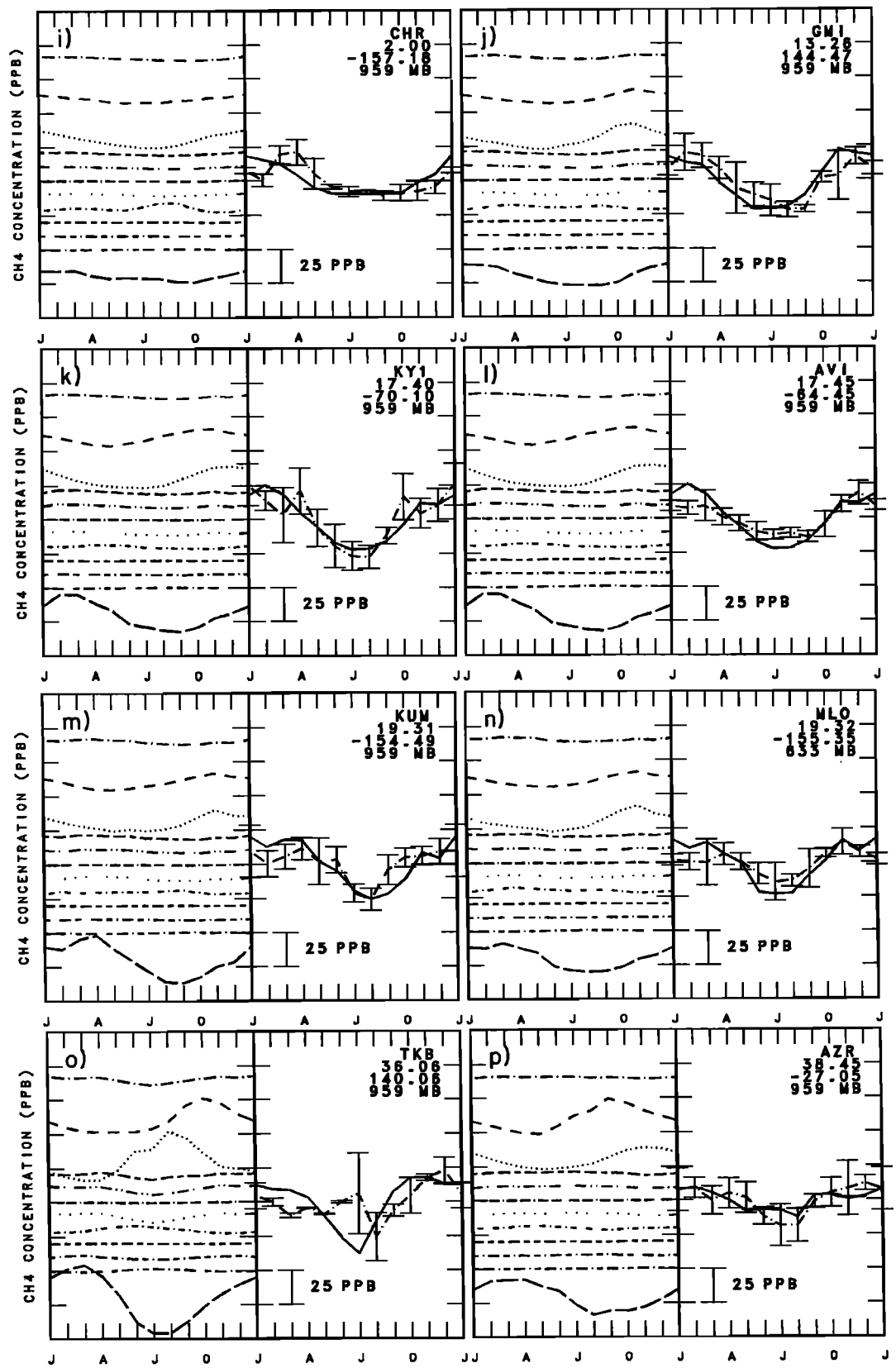

Fig. 7. (continued)

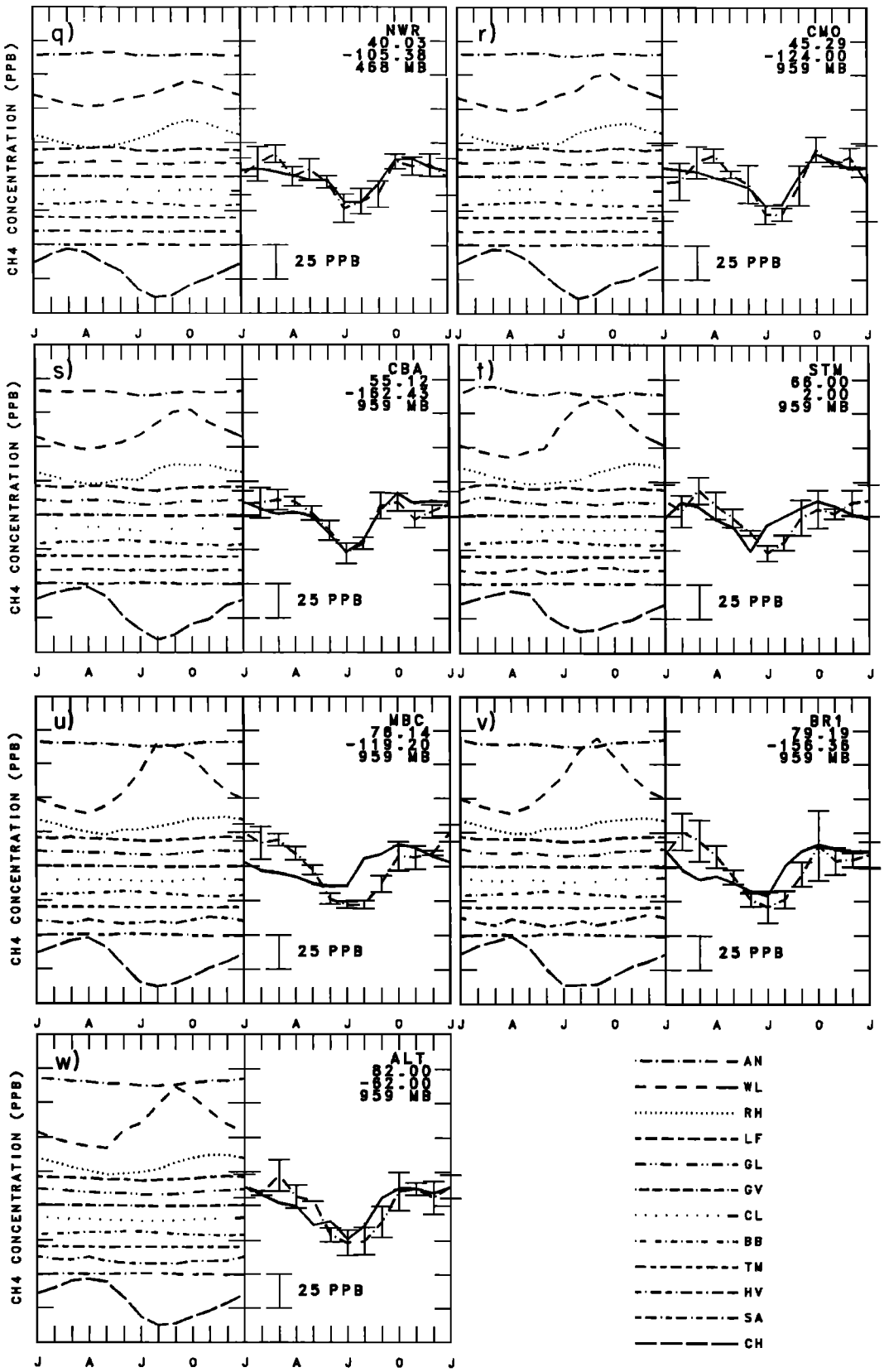

Fig. 7. (continued)

6 shows that the total tropical sources exceed 50% of the global sources: 315 Tg/yr in scenario 4 and 255 Tg/yr in scenario 7.

Further constraints on tropical sources are given by $\delta^{13}CH_4$. Fossil sources and biomass burning are the two methane sources that are heavier in $\delta^{13}CH_4$ than the atmosphere. And so, to maintain the $^{13}CH_4$ balance, an increase in the fossil fraction must be accompanied either by a decrease in the biomass burning source, or by a decrease in the $\delta^{13}C$ of the fossil sources themselves. The combinations (1) 100 Tg fossil fuel sources with $\delta^{13}C$ of -38 °/oo, and 80 Tg biomass burning source with $\delta^{13}C$ of -25 °/oo and (2) 100 Tg fossil fuel source with $\delta^{13}C$ of -42 °/oo, and 50 Tg biomass burning source with $\delta^{13}C$ of -27 °/oo would have comparable effects on the north-south gradient and $\delta^{13}CH_4$ balance. For a total global source strength of 500 Tg the biomass burning source ranges from 10 to 20% of the global sources, depending on the fossil fraction and on the $\delta^{13}C$ of the sources. The discussion above suggested a preferred a global fossil source fraction of 16% (scenarios 4 and 7), thus implying a biomass burning fraction of ~10%, comparable to that estimated for 1980 by *Craig et al.* [1988] and in the middle of the range estimated by *Quay et al.* [1991].

We included in the analysis atmospheric methane data from two sites proximate to the tropical sources: JBR (13°S) in Australia and TKB (36°N) in Japan. At these two sites the seasonal cycles are reasonably well simulated in all the budget scenarios. In particular, TKB, in the influence of the rice-growing regions of South and Southeast Asia, registers an annual mean concentration that is ~135 ppbv higher than that at SPO in both scenarios 4 and 7. Direct comparison with the observations is not strictly valid, as there is as yet no intercalibration of the methane data between TKB and the NOAA/CMDL network. However, the modeled difference between these two sites is within 20 ppbv of that derived from the observations, suggesting a global emission from rice paddies of ~100 Tg/yr. Intercalibration of the atmospheric data would facilitate an improvement in this estimate.

The remainder of the tropical sources, tropical wetlands and termites, are similar in that they have little impact on the atmospheric north-south gradient, and the measured ranges in their $\delta^{13}C$ overlap. In scenario 7 the simulated annual mean concentration is higher than that observed at CHR (2°N) by ~25 ppbv and at SMO (14°S) by ~10 ppbv (Figure 5). These overestimates may be caused by known uncertainties in the tropical meteorology in the GCM. They may also be due to uncertainties in the calculated OH distributions: similar overestimates of CH_3CCl_3 at SMO (14°S) result with the scaling factor employed here [*Spivakovsky et al.*, 1990*b*]. In other words, the model overestimate cannot be used to infer information about emissions from tropical wetlands or termites.

In scenarios 4 and 7 the emissions from tropical swamps were practically the same: 60 and 80 Tg/yr, respectively. The averaged fluxes implied by these source strengths are within the reported ranges (cf. Table 3). Because the representativeness of the fluxes cannot be assessed with so few measurements, we can only consider the magnitudes of these sources as not unreasonable.

Wahlen et al. [1989] placed an upper limit of ~130 Tg/yr on the combined emission from ruminants and termites. The limit is closely tied to, inter alia, $\delta^{13}C$ values used for the other sources and the $(k_{13}/k_{12})_{OH}$ value of *Davidson et al.* [1987]. In the scenarios we presented we selected $\delta^{13}CH_4$ values from within the ranges measured without making any judgments about the global representativeness of the measurements. The termite source is 100 and 20 Tg/yr in scenarios 4 and 7, respectively. As can be seen in Figures 2*l* and 3*c*, this source is assumed to be widespread and therefore produces a very dilute signature in the atmosphere and is one of the most difficult sources to constrain with the available atmospheric and in situ measurements.

The above discussion suggests that both scenarios 4 and 7 not only satisfy all constraints imposed by the atmospheric methane variations, but are consistent with the available direct estimates of the surface sources. There are two important differences between the two scenarios besides the chemical destruction rate. The first is the landfill source, whose magnitude is used to match the north-south gradient once the fossil fuel sources are specified. The second is the combined emissions from tropical wetlands and from termites, 160 and 100 Tg/yr in scenarios 4 and 7, respectively. There are not enough direct flux measurements from landfills and swamps to distinguish between the two scenarios. The conclusions of *Rasmussen and Khalil* [1983*a*, *b*], *Seiler et al.* [1984], *Fraser et al.* [1986*b*], and others would support scenario 7 with a small termite source. Also, recent measurements of slower rates of chemical reaction between OH and CH_4, leading to the suggestion of a longer atmospheric lifetime for methane [*Vaghjiani and Ravishankara*, 1991], would favor scenario 7.

7. THREE-DIMENSIONAL DISTRIBUTION OF METHANE IN THE ATMOSPHERE

Figure 8 shows the longitude-latitude distribution of $\phi(\lambda,\theta)$, the annual mean methane variations at ~960 mbar defined relative to the global annual mean concentration as simulated in scenario 7. Methane concentrations are elevated above the global annual mean in the northern hemisphere which provides ~75% of the sources. In North America, landfills, coal mining, natural gas pipeline leakage, and to a lesser degree the animal source are concentrated in the northeast, so that peak methane concentration there is ~100 ppbv above the global mean. High concentrations, also >100 ppbv above the global mean, are found in Central Europe and the USSR where the main sources are animals, landfills, and natural gas loss from both exploration and transmission. Similarly, concentration peaks of >100 ppbv are found over regions with intense rice cultivation and animal populations in China, India, and Bangladesh. Because we have assumed a clathrate source of 5 Tg/yr in the Soviet Arctic, the modeled concentration there shows a local maximum of 10–20 ppbv above the surrounding region, or ~120 ppbv above the global mean.

Concentrations are lower over oceanic regions than continental source regions. The difference is as large as ~50 ppbv in mid-latitudes in the northern hemisphere. A difference of a similar magnitude is also found around 30°S between the wetlands and animals of South America and the surrounding oceans.

It is difficult to anticipate the vertical distribution of methane in the atmosphere as the major source and sink terms all maximize near the surface: a surface source would contribute to a negative vertical gradient with methane decreasing with height, while a surface sink would lead to a positive gradient. We show in Figure 9 the concentration difference in the lower troposphere between layer 5 (~500 mbar) and layer 1 (Figure 9*a*), and in the upper troposphere between layer 7 (~200 mbar) and layer 5 (Figure 9*b*) of the atmospheric tracer model for scenario 7. At and above ~500 mbar, the concentrations are

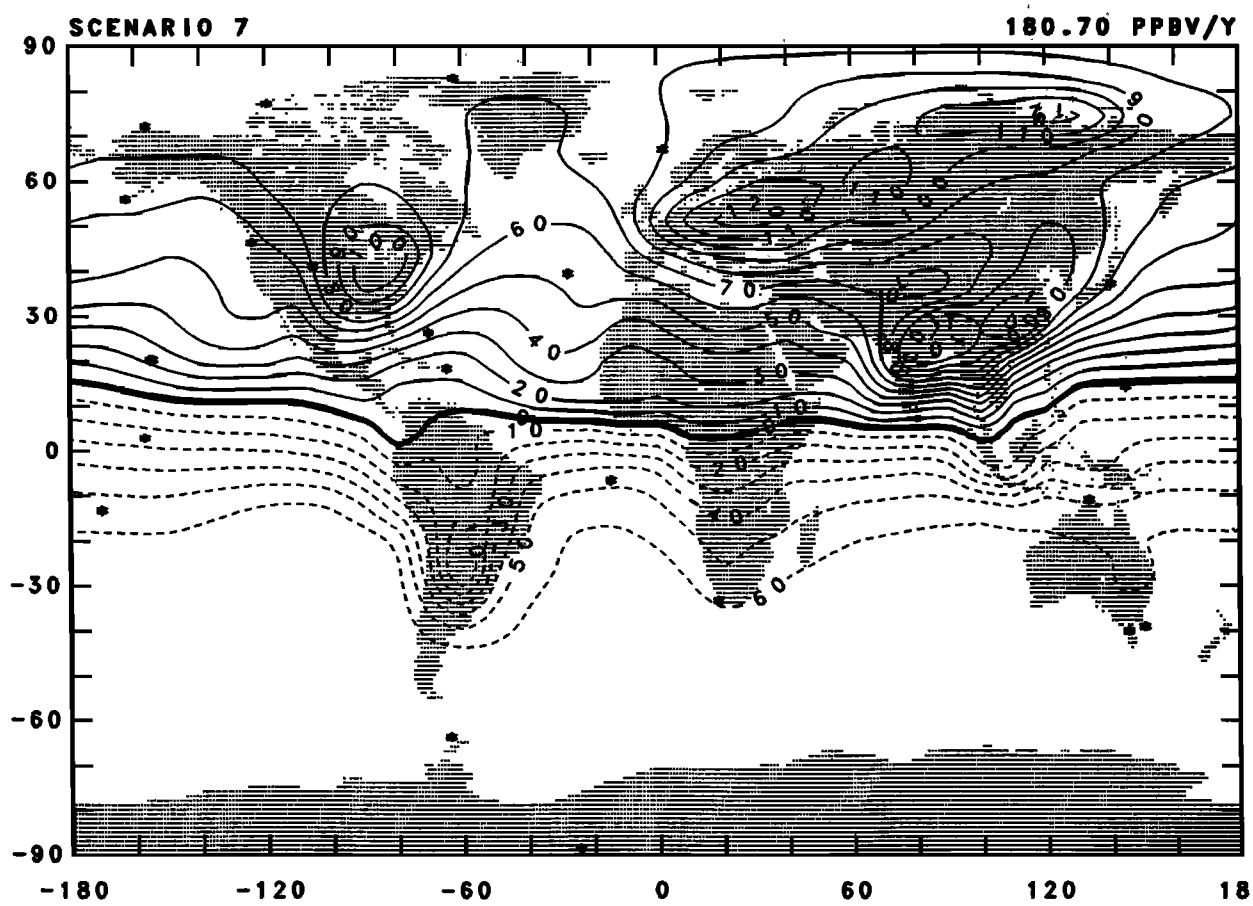

Fig. 8. Latitude-longitude distribution of the annual mean methane concentration $\phi(\lambda,\theta)$ ~960 mbar for scenario 7. Concentrations are defined relative to the global annual mean, and dashed lines denote negative values. Stars identify measurement locations listed in Table 1. Unit is ppbv.

relatively well mixed longitudinally, so that the pattern of vertical gradients below ~500 mbar resembles that of the surface concentration. Methane decreases with height in the lower troposphere (Figure 9a) over both continental and oceanic regions in the northern hemisphere and over the continental source regions in the southern hemisphere. At these places, emissions from the surface, spread out by the circulation, dominate over chemical destruction in the determination of the vertical profile. The largest attenuation is ~60 ppbv in the ~460 mbar layer between ~960 and ~500 mbar over the source regions, and is extremely weak, only ~10 ppbv in ~460 mbar, over the North Atlantic and Pacific.

Over the oceans in the southern hemisphere, chemical destruction is the only active source/sink term. In the absence of other processes, this would result in a vertical profile that increases with height. The vertical profile is modulated by source signals advected longitudinally from the continents and latitudinally from the northern hemisphere. In the lower troposphere over the southern oceans, these other processes are too weak to counter the chemical signal. This results in a vertical gradient opposite to that over the source regions: methane increases with height in the lower troposphere by 5–15 ppbv.

In most of the upper troposphere (Figure 9b), the sign of the methane vertical gradient is similar to that of the lower troposphere: concentrations decrease with height by 10–20 ppbv in ~200 mbar in the northern hemisphere and increase with height by ~10 ppbv in ~200 mbar in the southern hemisphere. An interesting exception is over the continental source regions in the southern hemisphere where the vertical concentration gradient changes sign from that in the lower troposphere. Here and elsewhere in the southern hemisphere, northern hemisphere methane is advected aloft across the equator and enhances the concentration increase caused by less effective OH destruction with height. Thus the vertical gradient is steeper in the upper than in the lower troposphere in the southern hemisphere. Figure 9b shows also a large decrease of methane over Greenland and Antarctica. This is an artifact of using concentrations at layer 7, which represent in these regions stratospheric air with very low methane concentrations.

There are very few methane profiles to support the modeled vertical distributions. The only long time series aircraft data available for the period of investigation here are the CSIRO aircraft data over Southeast Australia [*Fraser et al.*, 1986*a*]. The data show that, averaged over 1979–1984, the annual mean concentration of methane increases by ~6 ppbv from the surface to 3.5–5.5 km, and by another ~9 ppbv from 3.5–5 to ~7–10 km. This is in reasonable agreement with the modeled increases of ~5 and ~10 ppbv shown in Figures 9a and 9b, respectively. Similarly, the seasonal variations of the vertical profile over Southeast Australia are also realistically modeled (Figure 10). Like the observations reported by *Fraser et al.* [1986*a*], the steepest model gradient is found in February when methane increases nearly linearly from 80 ppbv below the global annual mean near the surface to 64 ppbv below the global annual mean at 300 mbar. The increase sharpens near

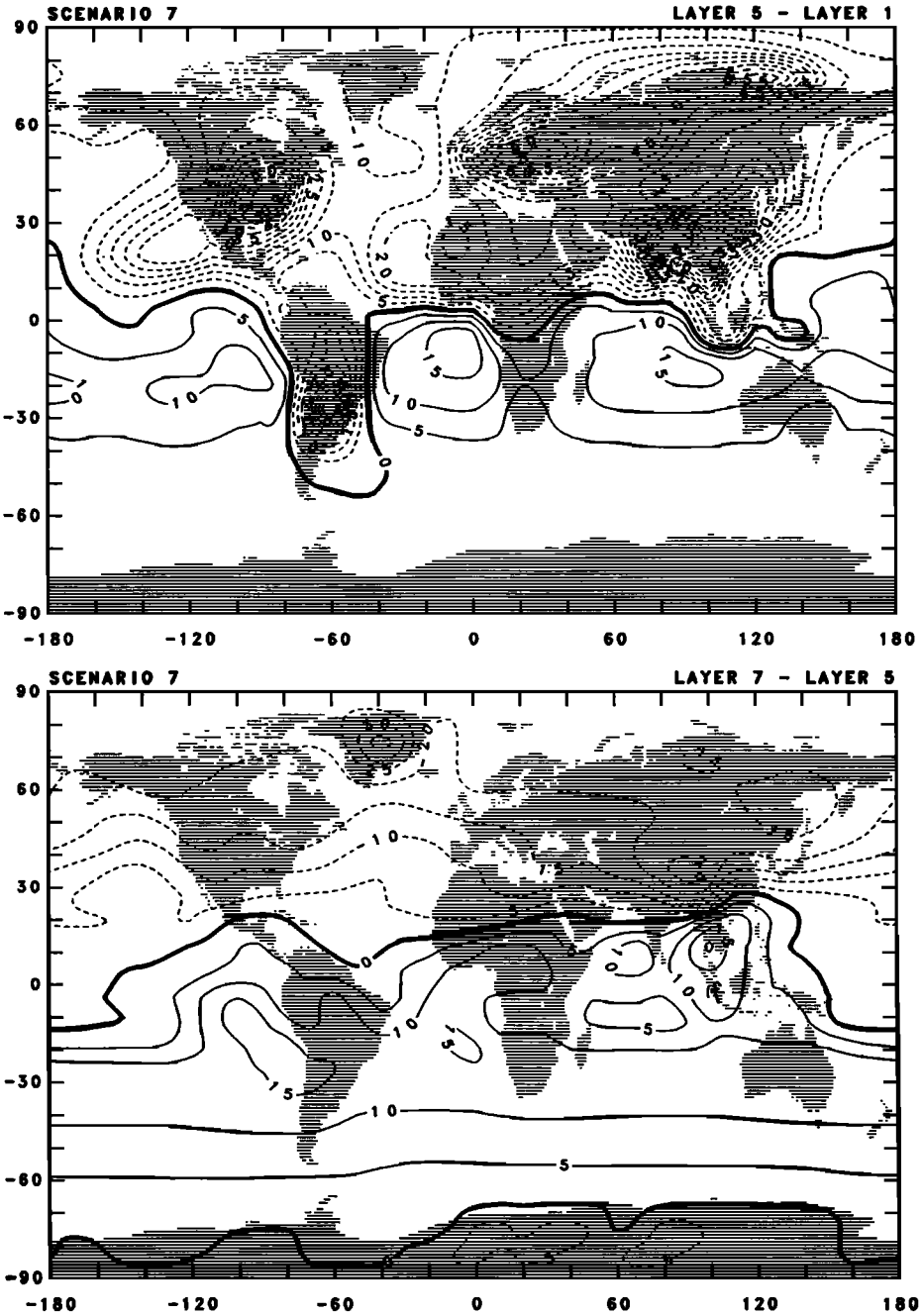

Fig. 9. Latitude-longitude distribution of the annual mean methane concentration differences simulated for scenario 7 (*a*) between layer 5 (~500 mbar) and layer 1 (~960 mbar), and (*b*) between layer 7 (~200 mbar) and layer 5. Dashed lines denote negative values. Unit is ppbv.

the tropopause, from 64 ppbv to 54 ppbv below the global annual mean from 300 to 200 mbar, respectively. The model indicates virtually no vertical gradient below 300 mbar in August. The modeled peak-trough seasonal amplitude decreases with height; at ~5 km it is ~60% of that at the surface and becomes insignificant near the tropopause.

While the NOAA/CMDL flask data from the two Hawaiian sites of MLO (20°N) and KUM (20°N) do not strictly represent the determination of a vertical profile in CH_4, they do lend valuable support to the modeled vertical distribution shown in Figure 9*a*. The site of KUM (20°N) is at sea level, while MLO (20°N) is at an elevation of 3397 m. Air samples are typically collected at MLO during downslope winds and are thought to represent free tropospheric methane concentrations. The measurements show annual average concentrations at MLO to be ~20 ppbv lower than at KUM [see Table 2; *Rasmussen and Khalil*, 1981*b*; *Steele et al.*, 1987]. The NOAA/CMDL data also suggest that there is a seasonal variation in the difference in concentration between KUM and MLO [*Steele et al.*, 1987]. The modeled vertical gradient for scenario 7 shown in Figure 9*a* shows a decrease of ~15 ppbv from layer 1 to layer 5 in the vicinity of these Hawaiian sites.

Between 1965 and 1967, *Ehhalt and Heidt* [1973] measured vertical profiles of tropospheric and stratospheric methane at

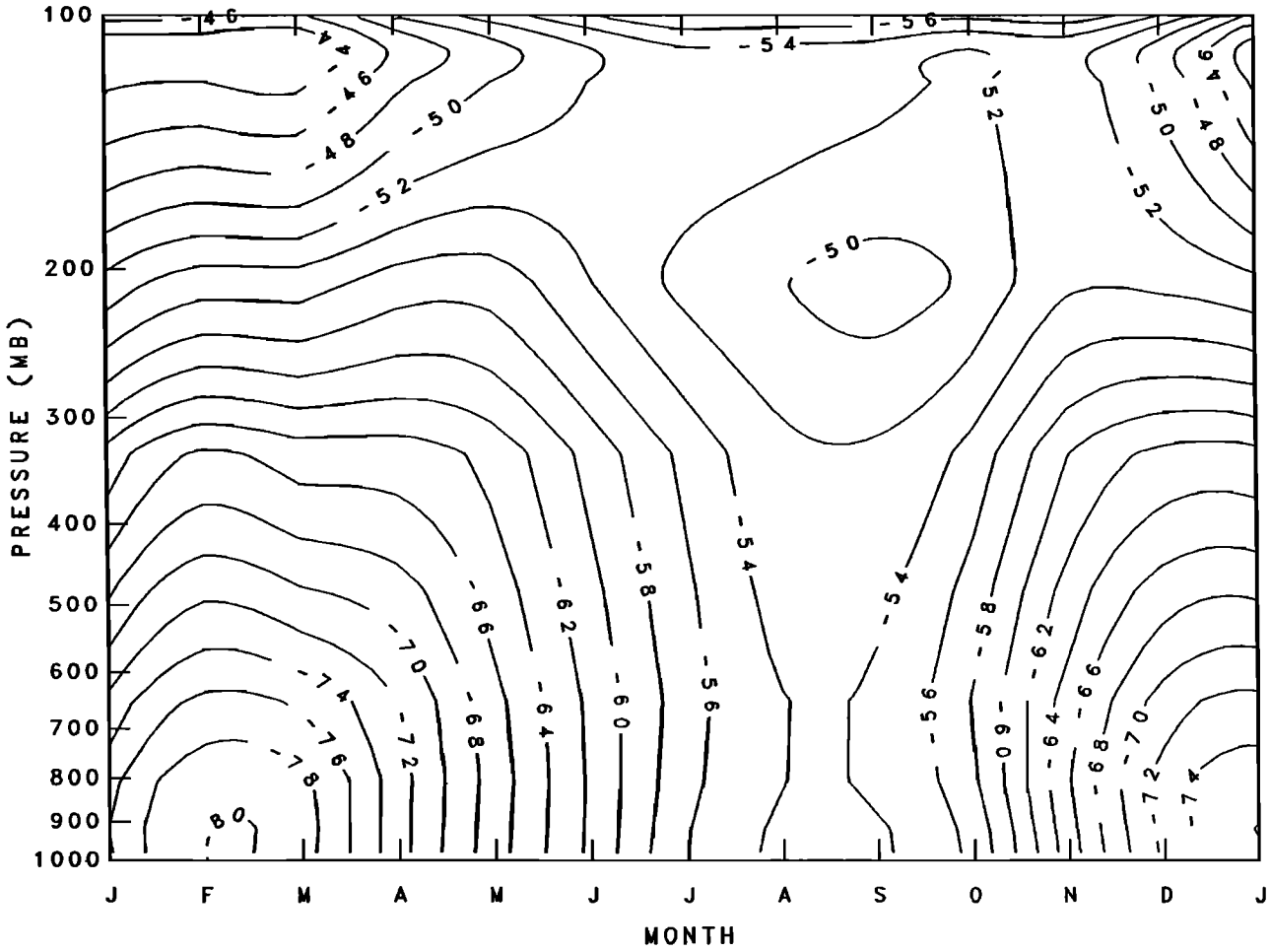

Fig. 10. Distribution of the seasonal and vertical variations of the methane concentration simulated at CGO. Concentrations are defined relative to the global annual mean. Unit is ppbv.

two locations: 200 km seaward of Santa Barbara, California, and at Scottsbluff, Arizona. Averaged over the year, tropospheric methane concentrations showed no significant vertical gradient (within ±30 ppbv) except for a slight decrease below 1 km. Similarly, no significant seasonal cycle in tropospheric methane was detected even though there were large fluctuations in individual profiles. Model results for the 1980s cannot be compared directly with measurements made two decades earlier when many of the present-day North American sources (landfills, natural gas consumption) likely played a smaller role in the methane budget. However, qualitative similarities are found between *Ehhalt and Heidt's* [1973] profiles and present-day profiles simulated over weak source regions in the southern hemisphere. This suggests that clues to the competition between increasing sources and decreasing chemical destruction in determining the secular trend of methane are contained in the secular trend of the vertical profiles, as the former would make the profile more negative and vice versa.

8. SUMMARY AND CONCLUSION

We have presented a comprehensive synthesis of our knowledge about the sources and sinks of methane and an analysis of the present-day global methane budget using constraints imposed by the variations of methane in the atmosphere. The primary objective of the work is to see if a global methane budget consistent with all available observations can be derived. If not, it is important to optimitize an observations strategy to improve our understanding of the methane cycle.

We first separated the problem of surface sources/sinks into two: one concerning the locations of the sources/sinks and the other concerning the magnitude of methane fluxes from each location.

Detailed mapping of the locations of the sources and sinks was carried out using available information on vegetation, soils, land use, and economic statistics. The most important natural source is wetlands, and our previous work presented a detailed compilation of wetland distribution using vegetation, soils, and inundation information. Because of their economic importance, the distribution of rice cultivation areas, animal populations, coal mines, and natural gas wells can be derived from national and global land use and energy atlases and statistics. Similarly, we assumed that landfill sizes and natural gas consumption within a country or political unit are proportional to the human population density within the unit and thus can be mapped using the distribution of population density. We consider these distributions to be fairly well known, although we have no measure to express our confidence quantitatively. While it is generally acknowledged that biomass burning occurs mainly in

the tropics, the areal extent, intensity and other characteristics of the fires are not known on a global, annual basis. We assumed that this source is colocated with the sources of CO_2 from deforestation and land-use modification. The information on termite populations and soil absorption is highly speculative, and these sources/sinks are crudely mapped based on their association with vegetation.

Over half of the surface sources/sinks were assumed to be constant through the year. For the seasonal sources the timing of the emissions was either derived directly from available statistics (rice cultivation) or modeled using climate information (wetlands, biomass burning).

There are far from enough field measurements to attempt a specification, on a global basis, of the magnitude and timing of the methane fluxes at each location for each source/sink. The only possible exception is emissions from ruminants and other domestic animals. Because methane production in these animals is considered energy wastage in commercial animal husbandry, methane fluxes from animals, at least in developed economies, are among the best known in the methane cycle. For the remainder of the surface sources and sinks we assumed values for the global annual source/sink strengths and tested how these values combine together to satisfy the constraints of mass balances, and to produce, in a three-dimensional atmospheric tracer transport model, concentration variations in the atmosphere that resemble those observed. The strengths of the sources and sinks are thus interdependent, and are determined from the combined signatures in the atmosphere.

The primary sink for methane is chemical destruction, and was modeled using four-dimensional OH fields derived by *Spivakovsky et al.* [1990*a*, *b*], who validated the fields by a simulation of atmospheric CH_3CCl_3. Uncertainties in the rate coefficient for the methane destruction affect conclusions about the lifetime and budget of methane. We used the 1990 JPL Panel evaluation of rate coefficients in the calculation, but examined the global budget taking into account uncertainties in the calculated OH fields as well as recent laboratory measurements of the reaction rate coefficent for OH with CH_4 *Vaghjiani and Ravishankara* [1991].

The methane budget cannot be uniquely defined using the data currently available. We presented six global methane budget scenarios that appear to satisfy all the constraints imposed by the atmospheric observations. While a single scenario cannot be selected objectively from the suite, we prefer scenarios with a low fraction of fossil sources as we demand that surface fluxes implied by a particular source strength are within reasonable bounds established directly from the statistics on emissions. It turns out that this choice hinges critically on the amount of methane vented at natural gas wells, a term for which there are no direct measurements. The low fossil fraction is consistent with the direct estimates of *Barns and Edmonds* [1990] who also found very little information on the uncombusted fraction of methane vented and flared at wells. Thus while we have a preferred budget scenario, the supporting evidence for some of the terms is weak and the scenario may be revised when we learn more about the treatment and fate of natural gas at the wells.

In summary, we prefer scenario 7 as the most likely budget. This scenario comprises an annual destruction of 450 Tg by OH oxidation and 10 Tg by soil absorption, and an annual emission of 80 Tg from fossil sources, 80 Tg from domestic animals, and 35 Tg from wetlands and tundra poleward of 50°N. Emissions from landfills, tropical swamps, rice fields, biomass burning, and termites total 295 Tg; however, the individual contributions of these terms cannot be determined uniquely. This budget is preferred for the following reasons. First, the methane lifetime corresponds to a CH_3CCl_3 lifetime of 6.3 yr [*Prinn et al.*, 1987] and is consistent with the lower rate coefficient derived recently by *Vaghjiani and Ravishankara* [1991]. Second, the total ^{14}C–free emission, the lowest of all the scenarios investigated, is consistent with that from direct estimates, even though the direct estimates are based on very sparse information. Third, we note that this scenario also matches successfully the north-south and seasonal variation of $\delta^{13}CH_4$ in the atmosphere reported by *Quay et al.* [1991].

Large uncertainties exist, in particular, about tropical and subtropical sources (rice, biomass burning, swamps, and termites), which make up >50% of the total sources. Data available as yet are too scanty to be organized into any systematic framework to quantify emissions on a global scale: the measured fluxes span orders of magnitude, and there is no clear way to rank the different factors found to impact emissions.

The analysis suggests a priority of measurements for defining and refining a global methane budget:

1. OH oxidation of methane in the troposphere is the largest single term in the global methane budget; it defines the total source strength. Narrowing the uncertainties in the magnitude and distribution of this term must be of prime importance. This would involve further refinements in the OH field through theoretical investigation, better definition of the climatologies of the atmospheric parameters and chemical species that affect OH, field experiments measuring OH concentrations under a range of atmospheric conditions, and further validation of the derived OH field using tracers such as the new synthetic HCFCs and HFCs [*Prather and Spivakovsky*, 1990]. We prefer a destruction rate of 450 Tg/yr, yielding a chemical lifetime of 10.1 yr for methane, which is within the range inferred using methyl chloroform and consistent with the new evaluation of the rate coefficient for the reaction with OH [*Vaghjiani and Ravishankara*, 1991]. However, uncertainties in three-dimensional distributions of H_2O, O_3, and NO_x in the atmosphere might affect some of the conclusions presented here which relied on the geographic information. Similarly, our preferred budget used a single value [from *Cantrell et al.*, 1990] for the associated kinetic isotopic fractionation ratio $(k_{13}/k_{12})_{OH}$. Confirmation of this value and its lack of temperature dependence (especially at temperatures <273K) would give confidence to the analysis which followed from these values.

2. The ^{14}C content of atmospheric methane defines the methane input associated with our energy demands and hence a large portion of the north-south gradient of atmospheric methane. While the range of estimates of ^{14}C–free methane has narrowed in recent years, uncertainties in the fossil fraction of the sources remain large. Improvements in the accuracy of ^{14}C measurements and a characterization of the spatial variability and global representativeness of the $^{14}CH_4$ data are necessary for an improved budget.

3. There must be an expanded measurement program to understand the controls and causes of variability of the methane fluxes found in the tropics. This is particularly important for emissions from rice fields and from biomass burning, two terms likely to play an important role in the increasing abundance of methane in the atmosphere.

4. Because of the variability found in the direct

measurements of methane fluxes and the difficulties in extrapolating them globally, indirect approaches will continue to be useful for inferring information about sources and sinks. For this approach to work, an expanded program in direct flux measurements must be accompanied by an expanded program to measure the three-dimensional distribution of methane in the atmosphere. In this way, regional fluxes can be constrained in a manner similar to that presented here. Regions where measurements of boundary layer methane concentrations are sorely needed include: the emergent and established agricultural regions of South and Southeast Asia, the mid-latitude population centers, and the hypothesized region of clathrate destabilization in the Soviet Arctic. Also, we should begin to investigate what information about the competition between increasing sources and decreasing sinks can be extracted from the temporal changes of the vertical profile. An update of the *Ehhalt and Heidt* [1973] profiles and continuation of the South and Southeast Australian profiles are paramount.

The increasing trend in atmospheric methane was not the focus of study here. Increased emissions associated with food and energy demands of a growing population, and decreased cleansing capacity of OH in the troposphere are the prime candidates in causing the trend. Feedbacks between climate change and natural systems are also likely to impact the methane trend [e.g., *Khalil and Rasmussen*, 1989], as is evident in the glacial-interglacial fluctuations of methane deduced from ice core records [*Raynaud et al.*, 1988; *Stauffer et al.*, 1988; *Chappellaz et al.*, 1990]. In the coming decades, high-latitude warming is hypothesized to enhance clathrate destabilization as well as wetland and tundra emissions. At the same time, increased methane consumption due to the drying of soils [*Whalen and Reeburgh*, 1990*b*] or decreased consumption due to expansion of agricultural land [*Keller et al.*, 1990] must not be ignored.

Acknowledgments. It is a pleasure to acknowledge the innumerable number of colleagues who generously shared their knowledge and data and provided preprints of their articles and critical comments on the manuscript. P. Lang, K. Masarie, R. Martin, and L. Waterman assisted in the collection, analysis, and processing of the NOAA/CMDL methane data. The NOAA/CMDL methane measurements were carried out in part under the Radiatively Important Trace Species (RITS) component of the NOAA Climate and Global Change Program. S. Coram of CSIRO collected and analyzed most of the Bass Strait flask samples. B. Noller, Office of the Supervising Scientist, Alligator Rivers Region, Jabiru East Laboratory, Northern Territory, collected the air samples at Jabiru. S. B. Ross participated in early stages of this study as part of the 1985 Summer Institute on Planets and Climate at NASA/GISS. K. Schwartz and C. Koizumi typeset the manuscript. This work was also supported by NASA Biospherics Research Program, NASA Interdisciplinary Research Program, NASA Tropospheric Chemistry Program, the Goddard Director's Discretionary Fund, and by the Office of Strategic Planning of the U.S. Environmental Protection Agency.

REFERENCES

Aselmann, I., and P. J. Crutzen, Global distribution of natural freshwater wetlands and rice paddies, their net primary productivity, seasonality and possible methane emissions, *J. Atmos. Chem.*, *8*, 307-358, 1989.

Barns, D. W., and J. A. Edmonds, An evaluation of the relationship between the production and use of energy and atmospheric methane emissions, *Rep. TR047*, Carbon Dioxide Res. Prog., U.S. Dep. of Energy, Washington, D. C., 1990. (Available as *DOE/NBB-0088P*, Nat. Tech. Inf. Serv., Springfield, Va., 1990.)

Bartlett, K. B., P. M. Crill, D. I. Sebacher, R. C. Harriss, J. O. Wilson, and J. M. Melack, Methane flux from the central Amazonian floodplain, *J. Geophys. Res.*, *93*, 1571-1582, 1988.

Bell, P. R., Methane hydrate and the carbon dioxide question, in *Carbon Dioxide Review, 1982*, edited by W. C. Clark, pp. 401-406, Oxford University Press, New York, 1983.

Bingemer, H. G., and P. J. Crutzen, The production of methane from solid wastes, *J. Geophys. Res.*, *92*, 2181-2187, 1987.

Blake, D. R., Increasing concentrations of atmospheric methane, 1979-1983, Ph.D. thesis, 213 pp., Univ. of Calif. at Irvine, 1984.

Blake, D. R., and F. S. Rowland, World-wide increase in tropospheric methane, 1978-1983, *J. Atmos. Chem.*, *4*, 43-62, 1986.

Blake, D. R., and F. S. Rowland, Continuing world-wide increase in tropospheric methane, 1978-1987, *Science*, *239*, 1129-1131, 1988.

Blake, D. R., E. W. Mayer, S. C. Tyler, Y. Makide, D. C. Montague, and F. S. Rowland, Global increase in atmospheric methane concentrations between 1978 and 1980, *Geophys. Res. Lett.*, *9*, 477-480, 1982.

Born, M., H. Dörr, and I. Levin, Methane consumption in aerated soils of the temperate zone, *Tellus Ser. B*, *42*, 2-8, 1990.

Brunke, E. G., H. E. Scheel, and W. Seiler, Trends of tropospheric CO, N_2O and CH_4 as observed at Cape Point, South Africa, *Atmos. Environ.*, *24A*, 585-595, 1990.

Cantrell, C. A., R. E. Shetter, A. H. McDaniel, J. G. Calvert, J. A. Davidson, D. C. Lowe, S. C. Tyler, R. J. Cicerone, and J. P. Greenberg, Carbon kinetic isotope effect in the oxidation of methane by the hydroxyl radical, *J. Geophys. Res.*, *95*, 22,455-22,462, 1990.

Central Intelligence Agency, *Polar Regions Atlas*, 66 pp., Washington, D. C., 1978.

Central Intelligence Agency, *USSR Energy Atlas*, 79 pp., Washington, D. C., 1985.

Chameides, W. L., S. C. Liu, and R. J. Cicerone, Possible variations in atmospheric methane, *J. Geophys. Res.*, *82*, 1795-1798, 1977.

Chanton, J., G. Pauly, C. Martens, N. Blair, and J. Dacey, Carbon isotopic composition of methane in Florida everglades soils and fractionation during its transport to the troposphere, *Global Biogeochem. Cycles*, *2*, 245-252, 1988.

Chanton, J., P. Crill, K. Bartlett, and C. Martens, Amazon Capims (Floating Grassmats): A source of ^{13}C enriched methane to the troposphere, *Geophys. Res. Lett.*, *16*, 799-802, 1989.

Chappellaz, J., J. M. Barnola, D. Raynaud, Y. S. Korotkevich, and C. Lorius, Ice-core record of atmospheric methane over the past 160,000 years, *Nature*, *345*, 127-131, 1990.

Cicerone, R. J., and J. D. Shetter, Sources of atmospheric methane: Measurements in rice paddies and a discussion, *J. Geophys. Res.*, *86*, 7203-7209, 1981.

Cicerone, R. J., and R. Oremland, Biogeochemical aspects of atmospheric methane, *Global Biogeochem. Cycles*, *2*, 299-328, 1988.

Cicerone, R. J., J. D. Shetter, and C. Delwiche, Seasonal variation of methane flux from a California rice paddy. *J. Geophys. Res.*, *88*, 11,022-11,024, 1983.

Cofer, W. F. III, J. S. Levine, E. L. Winstead, P. J. LeBel, A. M. Koller, Jr., and C. R. Hinkle, Trace gas emissions from burning Florida wetlands, *J. Geophys. Res.*, *95*, 1865-1879, 1990.

Craig, H., C. C. Chou, J. A. Welhan, C. M. Stevens, and A. Engelkemeir, The isotopic composition of methane in polar ice cores, *Science*, *242*, 1535-1539, 1988.

Crill, P., K. Bartlett, J. Wilson, D. Sebacher, R. Harriss, J. Melack, S. MacIntyre, L. Lesack, and L. Smith-Morrill, Tropospheric methane from an Amazonian floodplain lake, *J. Geophys. Res.*, *93*, 1564-1570, 1988*a*.

Crill, P. M., K. B. Bartlett, R. C. Harriss, E. Gorham, E. S. Verry, D. I. Sebacher, L. Madzar, and W. Sanner, Methane flux from Minnesota peatlands, *Global Biogeochem. Cycles*, *2*, 371-384, 1988*b*.

Crutzen, P. J., and M. O. Andreae, Biomass burning in the tropics: Impact on atmospheric chemistry and biogeochemical cycles, *Science*, *250*, 1669-1678, 1990.

Crutzen, P. J., and L. T. Gidel, A two-dimensional photochemical model of the atmosphere 2: The tropospheric budgets of the anthropogenic chlorocarbons CO, CH_4, CH_3, Cl and the effect of various NO_x sources on tropospheric ozone, *J. Geophys. Res.*, *88*, 6641-6661, 1983.

Crutzen, P. J., L. E. Heidt, J. P. Krasnec, W. H. Pollock, and W. Seiler, Biomass burning as a source of atmospheric gases CO, H_2, N_2O, NO, CH_3Cl and COS, *Nature*, *282*, 253-256, 1979.

Crutzen, P. J., I. Aselmann, and W. Seiler, Methane production by domestic animals, wild ruminants, other herbivorous fauna, and humans, *Tellus Ser. B*, *38*, 271-284, 1986.

Darmstadter, J., L. Ayres, R. Ayres, W. Clark, P. Crosson, P. Crutzen, T. Graedel, R. McGill, J. Richards, and J. Tarr, Impacts of world development on selected characteristics of the atmosphere: An integrative approach, *Rep. ORNL/Sub/86-22033*, Oak Ridge Natl. Lab., Oak Ridge, Tenn., 1987.

Davidson, J. A., C. A. Cantrell, S. C. Tyler, R. E. Shetter, R. Cicerone, and J. Calvert, Carbon kinetic isotope effect in the reaction of CH_4 with HO, *J. Geophys. Res., 92*, 2195-2199, 1987.

DeMore, W. B., M. J. Molina, S. P. Sander, D. M. Golden, R. F. Hampson, M. J. Kurylo, C. J. Howard and A. R. Ravishankara, Chemical kinetics and photochemical data for use in stratospheric modeling, *JPL Publ. 87-41*, 1987.

Detweiler, R. P., and C. A. S. Hall, Tropical forest and the global carbon cycle, *Science, 239*, 42-47, 1988.

Devol, A. H., and J. E. Richey, Seasonal dynamics in methane emissions from the Amazon River floodplain to the troposphere, *J. Geophys. Res., 95*, 16,417-16,426, 1990.

Devol, A., J. Richey, W. Clark, S. King, and L. Martinelli, Methane emissions to the troposphere from the Amazon floodplain, *J. Geophys. Res., 93*, 1583-1592, 1988.

Dianov-Klokov, V. I., and L. N. Yurganov, Spectroscopic measurements of atmospheric carbon monoxide and methane, 2, Seasonal variations and longterm trends, *J. Atmos. Chem, 8*, 153-164, 1989.

Dianov-Klokov, V. I., L. N. Yurganov, E. I. Grechko, and A. V. Dzhola, Spectroscopic measurements of atmospheric carbon monoxide and methane, 1, Latitudinal distribution, *J. Atmos. Chem., 8*, 139-151, 1989.

Druyan, L. M., and D. Rind, Verification of regional climates of GISS GCM-Part 1: Winter, *NASA Tech. Mem., 100,695*, 1988.

Druyan, L. M., and D. Rind, Verification of regional climates of GISS GCM-Part 2: Summer, *NASA Tech. Mem., 100,722*, 1989.

Ehhalt, D. H., Methane in the global atmosphere, *Environment, 27*, 6-33, 1985.

Ehhalt, D. H., The atmospheric cycle of methane, *Tellus, 26*, 58-70, 1974.

Ehhalt, D. H., and L. E. Heidt, Vertical profiles of CH_4 in the troposphere and stratosphere, *J. Geophys. Res., 78*, 5265-5271, 1973.

Ehhalt, D. H., and U. Schmidt, Sources and sinks of atmospheric methane, *Pageoph., 116*, 452-463, 1978.

Espenshade, E. B., Jr., (Ed.), *Goode's World Atlas*, 16th ed., 368 pp., Rand McNally, New York, 1978.

Food and Agriculture Organization, *1984 FAO Production Yearbook*, vol. 37, Food and Agriculture Organization of the United Nations, Rome, 1985.

Fraser, P. J., M. A. K. Khalil, R. A. Rasmussen, and A. J. Crawford, Trends of atmospheric methane in the southern hemisphere, *Geophys. Res. Lett., 8*, 1063-1066, 1981.

Fraser, P. J., M. A. K. Khalil, R. A. Rasmussen, and L. P. Steele, Tropospheric methane in the mid-latitudes of the southern hemisphere, *J. Atmos. Chem., 1*, 125-135, 1984.

Fraser, P. J., P. Hyson, R. A. Rasmussen, A. J. Crawford, and M. A. K. Khalil, Methane, carbon monoxide and methylchloroform in the southern hemisphere, *J. Atmos. Chem., 4*, 3-42, 1986*a*.

Fraser, P. J., R. A. Rasmussen, J. W. Creffield, J. R. French, and M. A. K. Khalil, Termites and global methane - Another assessment, *J. Atmos. Chem., 4*, 295-310, 1986*b*.

Fung, I., Analysis of the seasonal and geographical patterns of atmospheric CO_2 distributions with a 3-D tracer model, in *The Global Carbon Cycle: Analysis of the Natural Cycle and Implications of Anthropogenic Alterations for the Next Century*, edited by J. R. Trabalka and D. E. Reichle, pp. 459-473, Springer-Verlag, New York, 1986.

Fung, I., K. Prentice, E. Matthews, J. Lerner, and G. Russell, Three-dimensional tracer model study of atmospheric CO_2: Response to seasonal exchanges with the terrestrial biosphere, *J. Geophys. Res., 88*, 1281-1294, 1983.

Fung, I., C. J. Tucker, and K. C. Prentice, Application of AVHRR vegetation index to study atmosphere-biosphere exchange of CO_2, *J. Geophys. Res., 92*, 2999-3016, 1987.

Graedel, T. E., and J. E. McRae, On the possible increase of the atmospheric methane and carbon monoxide concentrations during the last decade, *Geophys. Res. Lett., 7*, 977-979, 1980.

Hansen, J., G. Russell, D. Rind, P. Stone, A. Lacis, S. Lebedeff, R. Ruedy, and L. Travis, Efficient three-dimensional global models for climate studies: models I and II, *Mon. Weather. Rev., 111*, 609-662, 1983.

Hao, W. M., M. H. Liu, and P. J. Crutzen, Estimates of annual and regional releases of CO_2 and other trace gases to the atmosphere from fires in the tropics, based on the FAO statistics for the period 1975-1980, in *Fire in the Tropical Biota - Ecosystem Process and Global Challenges*, edited by J. G. Goldammer, pp. 440-462, Springer-Verlag, New York, 1990.

Harriss R. C., D. I. Sebacher, and F. P. Day, Jr., Methane flux in the Great Dismal Swamp, *Nature, 297*, 673-674, 1982.

Harriss, R. C., S. Wofsy, J. Garstang, E. Browell, L. Molion, R. McNeal, J. Hoell, R. Bendura, S. Beck, R. Navarro, J. Riley, and R. Snell, The Amazon Boundary Layer Experiment (ABLE IIA): Dry season 1985, *J. Geophys. Res., 93*, 1351-1360, 1988.

Heidt, L. E., J. P. Krasnec, R. A. Lueb, W. H. Pollock, B. E. Henry, and P. J. Crutzen, Longitudinal distributions of CO and CH_4 over the Pacific, *J. Geophys. Res., 85*, 7329-7336, 1980.

Heimann, M. M., C. D. Keeling, and I. Fung, Simulating the atmospheric carbon dioxide distribution with a three-dimensional tracer model, in *The Global Carbon Cycle: Analysis of the Natural Cycle and Implications of Anthropogenic Alterations for the Next Century*, edited by J. R. Trabalka and D. E. Reichle, pp. 16-49, Springer-Verlag, New York, 1986.

Hirota, M., H. Muramatsu, Y. Makino, M. Ikegami, and K. Tsutsumi, Gas-chromatographic measurement of atmospheric methane in Japan, *Atmos. Environ., 23*, 1835-1839, 1989.

Holzapfel-Pschorn, A., and W. Seiler, Methane emission during a cultivation period from an Italian rice paddy, *J. Geophys. Res., 91*, 11,803-11,814, 1986.

Houghton, R. A., R. D. Boone, J. R. Fruci, J. E. Hobbie, J. M. Melillo, C. A. Palm, B. J. Peterson, G. R. Shaver, G. M. Woodwell, B. Moore, D. L. Skole, and N. Myers, The flux of carbon from terrestrial ecosystems to the atmosphere in 1980 due to changes in land use: Geographic distribution of the global flux, *Tellus Ser. B, 39*, 122-139, 1987.

Isaksen, I. S. A., and Ø. Hov, Calculation of trends in the tropospheric concentration of O_3, OH, CO, CH_4 and NO_x, *Tellus Ser. B, 39*, 271-285, 1987.

Jacob, D. J., and M. J. Prather, Radon-222 as a test of convective transport in a general circulation model, *Tellus Ser. B, 42*, 118-134, 1990.

Jacob, D., M. Prather, S. Wofsy, and M. McElroy, Atmospheric distribution of ^{85}Kr simulated with a general circulation model, *J. Geophys. Res., 92*, 6614-6626, 1987.

Jones, R. L., and J. A. Pyle, Observations of CH_4 and N_2O by the NIMBUS 7 SAMS: A comparison with in situ data and two-dimensional numerical model calculations, *J. Geophys. Res., 89*, 5263-5279, 1984.

Keller, M., T. J. Goreau, S. C. Wofsy, W. A. Kaplan, and M. B. McElroy, Production of nitrous oxide and consumption of methane by forest soils, *Geophys. Res. Lett., 10*, 1156-1159, 1983.

Keller, M., W. A. Kaplan, and S. C. Wofsy, Emission of N_2O, CH_4, and CO_2 from tropical forest soils, *J. Geophys. Res., 91*, 11,791-11,802, 1986.

Keller, M., M. E. Mitre, and R. F. Stallard, Consumption of atmospheric methane in soils of central Panama: Effects of agricultural development, *Global Biogeochem. Cycles, 4*, 21-28, 1990.

Khalil, M. A. K., and R. A. Rasmussen, Sources, sinks, and seasonal cycles of atmospheric methane, *J. Geophys. Res., 88*, 5131-5144, 1983.

Khalil, M. A. K., and R. A. Rasmussen, Climate-induced feedbacks for the global cycles of methane and nitrous oxide, *Tellus, 41B*, 554-559, 1989.

Khalil, M. A. K., R. A. Rasmussen, and M. J. Shearer, Trends of atmospheric methane during the 1960s and 1970s, *J. Geophys. Res., 94*, 18,279-18,288, 1989.

Khalil, M. A. K., R. A. Rasmussen, M.-X. Wang, and L. Ren, Emissions of trace gases from Chinese rice fields and biogas generators: CH_4, N_2O, CO, CO_2, chlorocarbons, and hydrocarbons, *Chemosphere*, 20, 207-226, 1990.

King, S. L., P. D. Quay, and J. M. Lansdown, The $^{13}C/^{12}C$ kinetic isotope effect for soil oxidation of methane at ambient atmospheric concentrations, *J. Geophys. Res., 94*, 18,273-18,277, 1989.

Kvenvolden, K., Methane hydrates and global climate, *Global Biogeochem. Cycles, 2*, 221-230, 1988.

Lamontagne, R. A., J. W. Swinnerton, and V. J. Linnenbom, C_1-C_4 hydrocarbons in the North and South Pacific, *Tellus, 26*, 71-77, 1974.

Lang, P. M., L. P. Steele, R. C. Martin, and K. A. Masarie, Atmospheric methane data for the period 1983-1985 from the NOAA/CMDL global cooperative flask sampling network, *Tech. Mem., ERL CMDL-1*, Natl. Oceanic and Atmos. Admin., Boulder, Colo., 1990*a*.

Lang, P. M., L. P. Steele, and R. C. Martin, Atmospheric methane data for the period 1986-1988 from the NOAA/CMDL global cooperative flask sampling network, *Tech. Mem., ERL CMDL-2*, Natl. Oceanic and Atmos. Admin., Boulder, Colo., 1990*b*.

Lerner, J., E. Matthews, and I. Fung, Methane emission from animals: A global high-resolution database, *Global Biogeochem. Cycles, 2*, 139-156, 1988.

Logan, J., M. Prather, S. Wofsy, and M. McElroy, Tropospheric chemistry: A global perspective, *J. Geophys. Res., 86*, 7210-7254, 1981.

Mahlman, J. D., and W. J. Moxim, Tracer simulation using a global general circulation model: Results from a mid-latitude instantaneous source experiment, *J. Atmos. Sci., 35*, 1340-1376, 1978.

Manning, M. R., D. C. Lowe, W. H. Melhuish, R. J. Sparks, C. A. M. Brenninkmeijer, and R.C. McGill, The use of radiocarbon measurements in atmospheric studies, *Radiocarbon, 32*, 37-58, 1990.

Matthews, E., Global vegetation and land use: new high-resolution data bases for climate studies, *J. Climate Appl. Meteorol., 22*, 474-487, 1983.

Matthews, E., and I. Fung, Methane emission from natural wetlands: Global distribution, area, and environmental characteristics of sources, *Global Biogeochem. Cycles, 1*, 61-86, 1987.

Matthews, E., I. Fung, and J. Lerner, Methane emission from rice cultivation: Geographic and seasonal distribution of cultivated areas and emissions, *Global Biogeochem. Cycles, 5*, 3-24, 1991.

Mayer, E. W., D. R. Blake, S. C. Tyler, Y. Makide, D. C. Montague, and F. S. Rowland, Methane: Interhemispheric concentration gradient and atmospheric residence time, *Proc. Natl. Acad. Sci. USA, 79*, 1366-1370, 1982.

Moore, T., N. Roulet, and R. Knowles, Spatial and temporal variations of methane flux from subarctic/northern boreal fens, *Global Biogeochem. Cycles, 4*, 29-46, 1990.

Pinto, J., Y. Yung, D. Rind, G. Russell, J. Lerner, J. Hansen, and S. Hameed, A general circulation model study of atmospheric carbon monoxide, *J. Geophys. Res.*, 3691-3702, 1983.

Prather, M., and C. Spivakovsky, Tropospheric OH and the lifetimes of hydrochlorofluorocarbons, *J. Geophys. Res., 95*, 18,723-18,729, 1990.

Prather, M., M. McElroy, S. Wofsy, G. Russell, and D. Rind, Chemistry of the global troposphere: Fluorocarbons as tracers of air motion, *J. Geophys. Res., 92*, 6579-6613, 1987.

Prinn, R., D. Cunnold, R. Rasmussen, P. Simmonds, F. Alyea, A. Crawford, P. Fraser, and R. Rosen, Atmospheric trends in methyl chloroform and the global average for the hydroxyl radical, *Science, 238*, 946-950, 1987.

Quay, P., S. L. King, J. M. Lansdown, and D. O. Wilbur, Isotopic composition of methane released from wetlands: Implications for the increase in atmospheric methane, *Global Biogeochem. Cycles, 2*, 385-397, 1988.

Quay, P. D., S. L. King, J. Stutsman, D. O. Wilbur, L. P. Steele, I. Fung, R. H. Gammon, T. A. Brown, G. W. Farwell, P. M. Grootes, and F. H. Schmidt, Carbon isotopic composition of atmospheric CH_4: Fossil and biomass burning source strengths, *Global Biogeochem. Cycles, 5*, 25-47, 1991.

Rasmussen, R. A., and M. A. K. Khalil, Atmospheric methane (CH_4): Trends and seasonal cycles, *J. Geophys. Res., 86*, 9826-9832, 1981*a*.

Rasmussen, R. A., and M. A. K. Khalil, Differences in the concentrations of atmospheric trace gases in and above the tropical boundary layer, *Pure Appl. Geophys., 119*, 990-997, 1981*b*.

Rasmussen, R. A., and M. A. K. Khalil, Global production of methane by termites, *Nature, 301*, 700-702, 1983*a*.

Rasmussen, R. A., and M. A. K. Khalil, Reply to Zimmerman and Greenberg, *Nature, 301*, 355, 1983*b*.

Rasmussen, R. A., and M. A. K. Khalil, Atmospheric methane in the recent and ancient atmospheres: Concentration, trends, and interhemispheric gradient, *J. Geophys. Res., 89*, 11,599-11,605, 1984*a*.

Rasmussen, R. A., and M. A. K. Khalil, The atmospheric lifetime of methychloroform (CH_3CCl_3), *Tellus Ser. B, 36*, 317-332, 1984*b*.

Rathje, W. L., Rubbish!, *The Atlantic Monthly, 264*, 99-109, 1989.

Raynaud, D., J. Chappellaz, J. M. Barnola, Y. S. Korotkevich, and C. Lorius, Climatic and CH_4-cycle implications of glacial-interlgacial CH_4 change in the Vostok ice core, *Nature, 333*, 655-657, 1988.

Revelle, R., Methane hydrates in continental slope sediments and increasing atmospheric carbon dioxide, in *Changing Climates*, pp. 252-261, National Academy Press, Washington, D. C. , 1983.

Russell, G., and J. Lerner, A new finite differencing scheme for the tracer transport equation, *J. Appl. Meteorol., 20*, 1483-1498, 1981.

Rust, F. E., $\delta(^{13}C/^{12}C)$ of ruminant methane and its relationship to atmospheric methane, *Science, 211*, 1044-1046, 1981.

Sackett, W. M., and T. R. Barber, Fossil carbon sources of atmospheric methane, *Nature, 334*, 201, 1988.

Sass, R. L., F. M. Fisher, P. A. Harcombe, and F. T. Turner, Methane production and emission in a Texas rice field, *Global Biogeochem. Cycles, 4*, 47-68, 1990.

Schütz, H., and W. Seiler, Methane flux measurements: Methods and results, in *Exchange of Trace Gases between Terrestrial Ecosystems and the Atmosphere*, edited by M. O. Andreae and D. S. Schimel, pp. 209-228, John Wiley, New York, 1989.

Schütz, H., A. Holzapfel-Pschorn, R. Conrad, H. Rennenberg, and W. Seiler, A three-year continuous record on the influence of daytime, season, and fertilizer treatment on methane emission rates from an Italian rice paddy, *J. Geophys. Res., 94*, 16,405-16,416, 1989.

Schütz, H., W. Seiler, and H. Rennenberg, Soil and land use related sources and sinks of methane (CH_4) in the context of the global methane budget, in *Soils and the Greenhouse Effect*, edited by A. F. Bouwman, pp. 269-285, John Wiley, New York, 1990.

Sebacher, D. I., R. C. Harriss, K. B. Bartlett, S. M. Sebacher, and S. S. Grice, Atmospheric methane sources: Alaskan tundra bogs, an alpine fen, and a subarctic boreal marsh, *Tellus Ser. B, 38*, 1-10, 1986.

Seiler, W., R. Conrad, and D. Scharffe, Field studies of CH_4 emissions from termite nests into the atmosphere and measurements of CH_4 uptake by tropical soils, *J. Atmos. Chem., 1*, 171-187, 1984.

Seydlitz Weltatlas, Cornelsen & Schroedel, Geographische Verlagsgesellschaft, Berlin, 232 pp., 1984.

Shea, D., Climatological atlas: 1950-1979, Surface air temperature, precipitation, sea-level pressure, and sea-surface temperature (45°S-90°N), *Tech. Note NCAR/TN-269+STR*, Natl. Cent. for Atmos. Res., Boulder, Colo., 1986.

Sheppard, J. C., H. Westberg, J. F. Hopper, K. Ganesan, and P. Zimmerman, Inventory of global methane sources and their production rates, *J. Geophys. Res., 87*, 1305-1312, 1982.

Spivakovsky, C. M., S. C. Wofsy, and M. J. Prather, A numerical method for parameterization of atmospheric chemistry: Computation of tropospheric OH, *J. Geophys. Res., 95*, 18,433-18,439, 1990*a*.

Spivakovsky, C. M., R. Yevich, J. A. Logan, S. C. Wofsy, M. B. McElroy, and M. J. Prather, Tropospheric OH in a three dimensional chemical tracer model: An assessment based on observations of CH_3CCl_3, *J. Geophys. Res., 95*, 18,441-18,471, 1990*b*.

Statistics Canada, *Gas utilities; Transport and distribution systems, 1984, SIC 4611-4921*, 71 pp., Census of Manufacturers Section, Industry Division, Statistics Canada, Ottawa, 1986.

Stauffer, B., E. Lochbronner, H. Oeschger, and J. Schwander, Methane concentration in the glacial atmosphere was only half that of the preindustrial Holocene, *Nature, 332*, 812-814, 1988.

Steele, L. P., and P. M. Lang, Atmospheric methane concentrations - the NOAA/CMDL global cooperative flask sampling network, 1983-1988. Numeric Data Package (NDP-038), prepared by R.J. Sepanski, *Rep. ORNL/CDIAC-42*. Carbon Dioxide Inf. Anal. Cent., Oak Ridge Nat. Lab., Oak Ridge, Tenn., 1991.

Steele, L. P., P. J. Fraser, R. A. Rasmussen, M. A. K. Khalil, T. J. Conway, A. J. Crawford, R. H. Gammon, K. A. Masarie, and K. W. Thoning, The global distribution of methane in the troposphere, *J. Atmos. Chem., 5*, 125-171, 1987.

Steudler, P. A., R. D. Bowden, J. M. Melillo, and J. D. Aber, Influence of nitrogen fertilization on methane uptake in temperate forest soils, *Nature, 341*, 314-316, 1989.

Stevens, C. M., Atmospheric methane, *Chem. Geol., 71*, 11-21, 1988.

Stevens, C., and A. Engelkemeir, Stable carbon isotopic composition of methane from some natural and anthropogenic sources, *J. Geophys. Res., 93*, 725-733, 1988.

Stevens, C., and A. Engelkemeir, Trends of the carbon isotopic composition of atmospheric methane, in *Geophysical Monitoring for Climatic Change 17, Summary Report 1988*, edited by J. W. Elkins, 142 pp., U.S. Department of Commerce, Washington, D. C., 1989.

Stevens, C., and F. Rust, The carbon isotopic composition of atmospheric methane, *J. Geophys. Res., 87*, 4879-4882, 1982.

Sullivan, W. T., III, *Earth at Night*, Poster available from the Hansen Planetarium, Salt Lake City, Utah, 1985.

Svensson, B. H., Carbon dioxide and methane fluxes from the ombrotrophic parts of a subarctic mire, *Ecol. Bull. Stockholm, 30*, 235-250, 1980.

Svensson, B. H., and T. Rosswall, In situ methane production from acid peat in plant communities with different moisture regimes in a subarctic mire, *Oikos, 43*, 341-350, 1984.

Sze, N. D., Anthropogenic CO emissions: implications for the atmospheric CO-OH-CH_4 cycle, *Science, 195*, 673-675, 1977.

Tans, P. P., I. Y. Fung, and T. Takahashi, Observational constraints on the global atmospheric CO_2 budget, *Science, 247*, 1431-1438, 1990.

Taylor, J. A., G. Brasseur, P. Zimmerman, and R. Cicerone, A study of the sources and sinks of methane and methyl chloroform using a global three-dimensional Lagrangian tropospheric tracer transport model, *J. Geophys. Res., 96*, 3013-3044, 1991.

Thompson, A. M., and R. J. Cicerone, Atmosperic CH_4, CO and OH from 1960 to 1985, *Nature, 321*, 148-150, 1986.

Thornthwaite, C. W., An approach toward a rational classification of climate, *Geogr. Rev., 38*, 55-89, 1948.

Tyler, S. C., Stable carbon isotope ratios in atmospheric methane and some of its sources, *J. Geophys. Res., 91*, 13,232-13,238, 1986.

Tyler, S. C., P. R. Zimmerman, C. Cumberbatch, J. P. Greenberg, C. Westberg, and J. P. E. C. Darlington, Measurements and interpretation of $\delta^{13}C$ of methane from termites, rice paddies, and wetlands in Kenya, *Global Biogeochem. Cycles, 2*, 341-355, 1988.

Tyler, S. C., $^{13}C/^{12}C$ ratios in atmospheric methane and some of its sources, in *Stable Isotopes in Ecological Research*, vol 68, edited by P. W. Rundel, J. R. Ehleringer, and K. A. Nagy, pp. 395-409, Springer-Verlag, New York, 1989.

Tyler, S. C., D. C. Lowe, E. Dlugokencky, P. R. Zimmerman, and R. J. Cicerone, Methane and carbon monoxide emissions from asphalt pavement: Measurements and estimates of their importance to global budgets, *J. Geophys. Res., 95*, 14,007-14,014, 1990.

U.N. Department of International Economic and Social Affairs, *Energy Statistics Yearbook 1984*, 441 pp., United Nations, 1986.

U.S. Department of Energy, *International Energy Annual 1985, Rep. DOE/EIA-219(85)*, 129 pp., Energy Inf. Admin., Off. of Energy Markets and End Use, Washington, D. C., 1986*a*.

U.S. Department of Energy, *Natural Gas Annual 1985, Rep. DOE/EIA-0131(85)*, 280 pp., Energy Inf. Admin., Off. of Oil and Gas, Washington, D. C., 1986*b*.

Vaghjiani, G. R., and A. R. Ravishankara, New measurement of the rate coefficient for the reaction of OH with methane, *Nature, 350*, 406-408, 1991.

Wahlen, M., N. Tanaka, R. Henry, B. Deck, J. Zeglen, J. Vogel, J. Southon, A. Shemesh, R. Fairbanks, and W. Broecker, Carbon-14 in methane sources and in atmospheric methane: The contribution from fossil carbon, *Science, 245*, 286-290, 1989.

Whalen, S. C., and W. S. Reeburgh, A methane flux time-series for tundra environments, *Global Biogeochem. Cycles, 2*, 399-410, 1988.

Whalen, S. C., and W. S. Reeburgh, A methane flux transect along the trans-Alaska pipeline haul road, *Tellus Ser. B, 42*, 237-249, 1990*a*.

Whalen, S. C., and W. S. Reeburgh, Consumption of atmospheric methane by tundra soils, *Nature*, 346, 160-162, 1990*b*.

Whalen, S. C., W. S. Reeburgh, and K. A. Sandbeck, Rapid methane oxidation in a landfill cover soil, *Appl. Environ. Microbiol.*, in press, 1990.

Wilkness, P. E., R. A. Lamontagne, R. E. Larson, J. W. Swinnerton, C. R. Dickson, and T. Thompson, Atmospheric trace gases in the southern hemisphere, *Nature, 245*, 45-47, 1973.

Yagi, K., and K. Minami, Effects of organic matter applications on methane emission from Japanese paddy fields, in *Soils and the Greenhouse Effect*, edited by A. F. Bouwman pp. 467-474, John Wiley, New York, 1990.

Zander, R., Ph. Demoulin, D. H. Ehhalt, and U. Schmidt, Secular increase of the vertical column abundance of methane derived from IR solar spectra recorded at the Jungfraujoch station, *J. Geophys. Res., 94*, 11,021-11,028, 1989.

Zimmerman, P. R., and J. P. Greenberg, Termites and methane, *Nature, 302*, 354-355, 1983.

Zimmerman, P. R., J. P. Greenberg, S. O. Wandiga, and P. J. Crutzen, Termites: A potentially large source of atmospheric methane, carbon dioxide and molecular hydrogen, *Science, 218*, 563-565, 1982.

Zimmerman, P. R., J. P. Greenberg, and J. P. E. C. Darlington, Response to Termites and atmospheric gas production (technical comment by N.M. Collins, and T.G. Wood), *Science, 224*, 84-86, 1984.

Zobler, L., A world soil data file for global climate modeling, *NASA Tech. Mem. 87802*, 32 pp., 1986.

P. J. Fraser and L. P. Steele, CSIRO Division of Atmospheric Research, Private Bag No. 1, Mordialloc, Victoria 3195, Australia.

I. Fung and M. Prather, NASA Goddard Space Flight Center, Institute for Space Studies, 2880 Broadway, New York, New York 10025.

J. John, Department of Applied Physics, Columbia University, New York, New York 10027.

J. Lerner and E. Matthews, STX Corporation, 2880 Broadway, New York, New York 10025.

(Received July 20, 1990;
revised April 30, 1991;
accepted April 30, 1991.)